General Disclaimer

One or more of the Following Statements may affect this Document

- This document has been reproduced from the best copy furnished by the organizational source. It is being released in the interest of making available as much information as possible.

- This document may contain data, which exceeds the sheet parameters. It was furnished in this condition by the organizational source and is the best copy available.

- This document may contain tone-on-tone or color graphs, charts and/or pictures, which have been reproduced in black and white.

- This document is paginated as submitted by the original source.

- Portions of this document are not fully legible due to the historical nature of some of the material. However, it is the best reproduction available from the original submission.

CHARACTERIZATION OF 8–cm ENGINEERING MODEL THRUSTER

W.S. Williamson

Hughes Research Laboratories
3011 Malibu Canyon Road
Malibu, CA 90265

March 1984

NAS3–21358
Final Report
12 April 1978 through 12 September 1982

NASA Lewis Research Center
21000 Brookpark Road
Cleveland, OH 44135

TECHNICAL REPORT STANDARD TITLE PAGE

1. Report No.	2. Government Accession No.	3. Recipient's Catalog No.
CR-174673		

4. Title and Subtitle	5. Report Date
CHARACTERIZATION OF 8-cm ENGINEERING MODEL THRUSTER	6. Performing Organization Code

7 Author(s)	8. Performing Organization Report No.
W.S. Williamson	

9. Performing Organization Name and Address	10. Work Unit No.
Hughes Research Laboratories 3011 Malibu Canyon Road Malibu CA 90265	11. Contract or Grant No. NAS3-21358, NAS3-21036

12. Sponsoring Agency Name and Address	13. Type of Report and Period Covered
NASA Lewis Research Center 21000 Brookpark Road Cleveland, OH 44135	Final Report Oct 1977 - Oct 1982
	14. Sponsoring Agency Code

15. Supplementary Notes

16. Abstract

We report development of 8-cm ion thruster technology which was conducted in support of the Ion Auxiliary Propulsion System (IAPS) flight contract (Contract NAS3-21055). The work included characterization of thruster performance, stability, and control; a study of the effects of cathode aging; environmental qualification testing; and cyclic lifetesting of especially critical thruster components.

17. Key Words (Selected by Author(s))	18. Distribution Statement
Electric Propulsion Mercury Ion Thruster Auxiliary Propulsion	

19. Security Classif. (of this report)	20. Security Classif. (of this page)	21. No. of Pages	22. Price*
UNCLASSIFIED	UNCLASSIFIED	85	

*For sale by the Clearinghouse for Federal Scientific and Technical Information, Springfield, Virginia 22151.

TABLE OF CONTENTS

LIST OF ILLUSTRATIONS

SYMBOLOGY

THE LISTING BELOW IDENTIFIES THE SYMBOLS USED IN THIS REPORT. THE SIGNIFICANCE OF ELECTRICAL QUANTITIES CAN BE SEEN IN THE SCHEMATIC DIAGRAM GIVEN IN FIGURE 3 IN SECTION 2.

BEAM VOLTAGE:	V_B
BEAM CURRENT:	I_B
ACCELERATOR VOLTAGE:	V_A
ACCELERATOR CURRENT:	I_A
SCREEN VOLTAGE:	V_S
SCREEN CURRENT:	I_S
DISCHARGE VOLTAGE:	V_D
DISCHARGE CURRENT:	I_D
DISCHARGE KEEPER VOLTAGE:	V_{DK}
DISCHARGE KEEPER CURRENT:	I_{DK}
KEEPER-TO-ANODE VOLTAGE:	V_δ $(= V_D - V_{DK})$
DISCHARGE VAPORIZER VOLTAGE:	V_{DV}
DISCHARGE VAPORIZER CURRENT:	I_{DV}
DISCHARGE CATHODE HEATER VOLTAGE:	V_{DH}
DISCHARGE CATHODE HEATER CURRENT:	I_{DH}
DISCHARGE CATHODE HEATER POWER	P_{DH}
NEUTRALIZER KEEPER VOLTAGE:	V_{NK}
NEUTRALIZER KEEPER CURRENT:	I_{NK}
NEUTRALIZER VAPORIZER VOLTAGE:	V_{NV}
NEUTRALIZER VAPORIZER CURRENT:	I_{NV}
NEUTRALIZER CATHODE HEATER VOLTAGE:	V_{NH}
NEUTRALIZER CATHODE HEATER CURRENT:	I_{NH}
NEUTRALIZER CATHODE HEATER POWER:	P_{NH}
NEUTRALIZER COUPLING CURRENT:	I_N
NEUTRALIZER COUPLING VOLTAGE:	V_N
DISCHARGE PROPELLANT FLOWRATE:	I_{DHg}
NEUTRALIZER PROPELLANT FLOWRATE:	I_{NHg}
TOTAL PROPELLANT FLOWRATE:	I_{Hg} $(= I_{DHg} + I_{NHg})$
DISCHARGE PROPELLANT UTILIZATION EFFICIENCY:	η'_{Hg} $(\approx I_B/I_{DHg})$
TOTAL PROPELLANT UTILIZATION EFFICIENCY:	η_{Hg} $(\approx I_B/(I_{DHg} + I_{NHg}))$
DISCHARGE SPECIFIC ENERGY:	ε_I $(= (V_D I_D + V_{DK} I_{DK})/I_B)$

SECTION 1

INTRODUCTION

This document reports work performed between October 1977 and October 1982 under two separate contracts from NASA Lewis Research Center (NASA LeRC): contracts NAS3-21036 and NAS3-21358. Because the subject material of the two efforts was closely related, we have incorporated the data from the earlier contract (NAS3-21036) into this final report for the later contract (NAS3-21358). This combined-report format has been approved by the NASA LeRC Technical Project Manager.

These contractual efforts have borne a close relationship to the Ion Auxiliary Propulsion System (IAPS) flight contract (contract NAS3-21055) in that they have had as their focus the thorough characterization and documentation of the IAPS 8-cm-ion-thruster technology. This work has also included the development of specific components and technologies for the IAPS where the pre-existing level of technology was deemed inadequate. These efforts have included characterization of the most critical elements of the 8-cm Engineering Model ion Thruster (EMT) and lifetesting of components for which durability is a reliability driver. In addition, system considerations such as the stability and response characteristics of the thruster/power-processor interface were investigated.

In many cases, the activities that we conducted under the subject programs were complementary to those carried out under the IAPS flight program. For example, several instances occurred in which our characterization testing revealed design modifications which could substantially improve specific characteristics of the 8-cm Flight Model Thruster (FMT); in several instances we designed and tested new components to satisfy these goals, and the components were successfully

integrated into the FMTs. Similarly, we participated in the development of the thruster-control algorithms that were recommended to the Flight Program, and we conducted investigations of the thruster-control software that resulted from these algorithms. At this writing, the IAPS units have successfully passed qualification and environmental testing, and we look forward to a successful outcome of the pending spaceflight test aboard a United States Air Force spacecraft.

SECTION 2

HARDWARE DESCRIPTION: 8-cm THRUSTER AND POWER PROCESSOR

In this section we provide a cursory description of the 8-cm thruster, the power-electronics unit (PEU) and the digital-controller-and-interface unit (DCIU). These elements underwent substantial design revision during the course of the subject efforts. In the interest of clarity, we will refer to the electronics (PEU and DCIU) in their flight-model versions, and we will distinguish only two versions of the thruster (flight-model and engineering-model thrusters). The assembly which consists of the thruster, gimbal, and beamshield will be referred to as the TGBSU.

A. 8-cm THRUSTER

Figures 1 and 2 show the Engineering-Model Thruster (EMT) and Flight-Model Thruster (FMT) system which were the principal subjects of this investigation. The drawings identify several specific differences which we will describe in detail in later sections.

The thrusters consist of a cylindrical Penning discharge chamber which is bounded axially by a cathode-potential endplate (at the upstream end) and a cathode-potential screen electrode (at the downstream end). A cylindrical anode bounds the interior of the discharge chamber radially. A divergent magnetic field emanates from the cathode polepiece (on the endplate) and passes downstream and radially outward to the screen polepiece (surrounding the screen electrode). The magnetic field is produced by 8 rod-shaped permanent magnets which are confined in tubes on the outside of the discharge-chamber shell. These magnet tubes are brazed to the flanges at each end of the discharge chamber, adding axial strength to the structure.

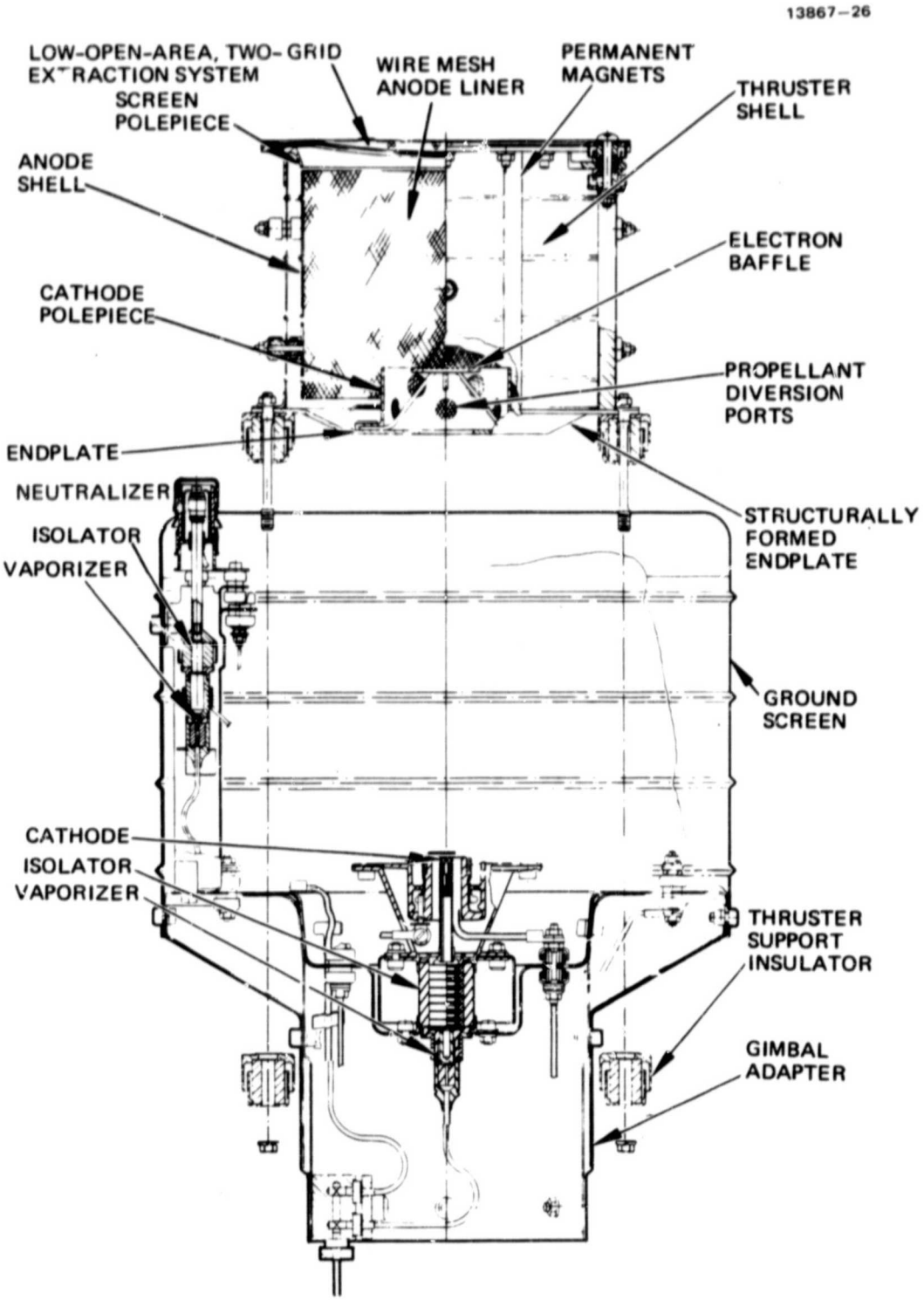

Figure 1. Engineering-model thruster.

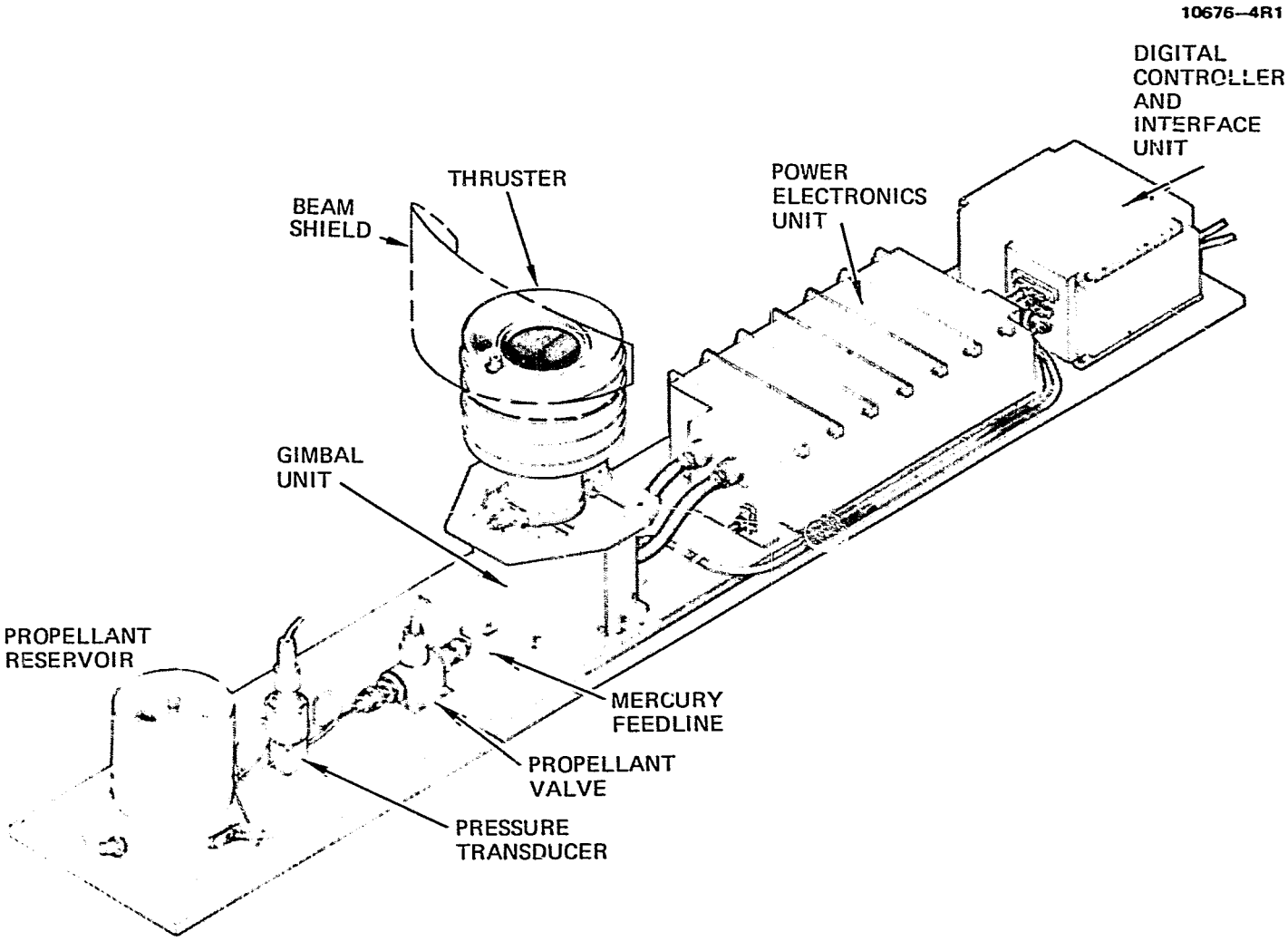

Figure 2. Flight-model thruster system.

Electrons are injected into the discharge chamber by a hollow cathode which is mounted through a hole penetrating the endplate. The cathode is surrounded by the cathode polepiece. A disk-shaped electron baffle is located downstream of the cathode, flush with the downstream surface of the cathode polepiece. The geometry of the electron baffle forces electrons to cross magnetic field lines before entering the discharge plasma; this geometry is responsible for maintaining a high potential difference (typically 25 V) between the plasma inside the cathode polepiece and the main discharge.

Propellant is supplied to the thruster from a remote blowdown propellant tank. A valve isolates the propellant tank from the thruster. When the valve is open, mercury propellant flows down the propellant line to a porous-tungsten vaporizer which is located at the upstream end of the unified cathode-isolator-vaporizer (CIV) structure. Liquid mercury is not normally able to penetrate the small (1.0-1.5-μm-diameter) pores of the porous-tungsten material, so the vaporizer acts as a phase separator, permitting only mercury vapor to pass through. The flowrate of mercury vapor that leaves the downstream side of the vaporizer is a strong, single-valued function of the vaporizer temperature, and this relationship is used to control propellant flowrate in the 8-cm thruster. The vaporizer temperature is monitored by a platinum resistance thermal device (RTD) which changes resistance as a function of temperature.

Mercury vapor that is produced in the vaporizer passes through an electrically insulating structure called the isolator, which consists of a stack of alternating alumina spacers and wire-mesh disks. The vaporizer side of this column is at spacecraft-ground potential, while the other end (discharge-chamber side) is at beam potential (1200 V). The design of the isolator allows for the passage of the mercury vapor without incurring Paschen breakdown.

Mercury vapor enters the discharge chamber through the discharge-cathode orifice; the majority of the vapor is ionized in the main discharge by primary-electron impact. Ions created in this discharge are extracted by a conventional two-grid ion-beam extraction system having a low-open-area accelerator grid (this design minimizes losses of un-ionized propellant without degrading ion-beam quality). An ion-beam current of 72 mA is the design operating point, providing a thrust of about 5 mN.

B. POWER ELECTRONICS UNIT (PEU)

Power is provided to the thruster and gimbal by the PEU, which is in turn controlled by a physically separate controller, the DCIU (described in the next section). The PEU consists of eleven separate power supplies for separate functions which are identified in Figure 3 and listed in Table 1. These power supplies include two keeper "ignitors", which deliver a higher-than-normal potential (approximately 500-V instead of 50-V) to the desired keeper to aid in ignition. The screen and accel supplies are controlled by on/off commands, and the keeper ignitors are also on/off in nature; all other supplies are controlled by 0-to-5-V analog signals which are generated in the DCIU. The PEU also generates 0-to-5-V telemetry signals which provide information to the DCIU about the status of power-supply outputs.

C. DIGITAL-CONTROLLER-AND-INTERFACE UNIT (DCIU)

The DCIU is the central control unit of the IAPS, providing capabilities to decode incoming commands and issue required

Table 1. Power Supplies in PEU

13867–14

POWER SUPPLY	SETPOINT NO.	VALUE	TYPE OF REGULATION
DISCHARGE VAPORIZER, DV	0 1 2 3 4 5 6	2.5 W 5.0 7.5 10.0 12.5 15.0 20.0	CURRENT
NEUTRALIZER VAPORIZER, NV	0 1 2 3	1.5 W 2.5 4.0 8.0	CURRENT
DISCHARGE CATHODE HEATER, DH	0 1 2 3 4 5 6 7	2 W 5 10 15 23 26 32 38	CURRENT
NEUTRALIZER CATHODE HEATER, NH	0 1 2 3 4 5 6 7	3 W 6 10 15 20 23 30 38	CURRENT
DISCHARGE KEEPER, DK	0 1 2 3	60 mA 120 360 500	CURRENT
NEUTRALIZER KEEPER, NK	0 1 2 3	300 mA 425 500 600	CURRENT
SCREEN	ON/OFF	1180 V	VOLTAGE
ACCEL	ON/OFF	-300 V	VOLTAGE
DISCHARGE	256 SETPOINTS	MAX 1 A	CURRENT
DISCHARGE KEEPER IGNITOR	ON/OFF	550 V	VOLTAGE
NEUTRALIZER KEEPER IGNITOR	ON/OFF	550 V	VOLTAGE

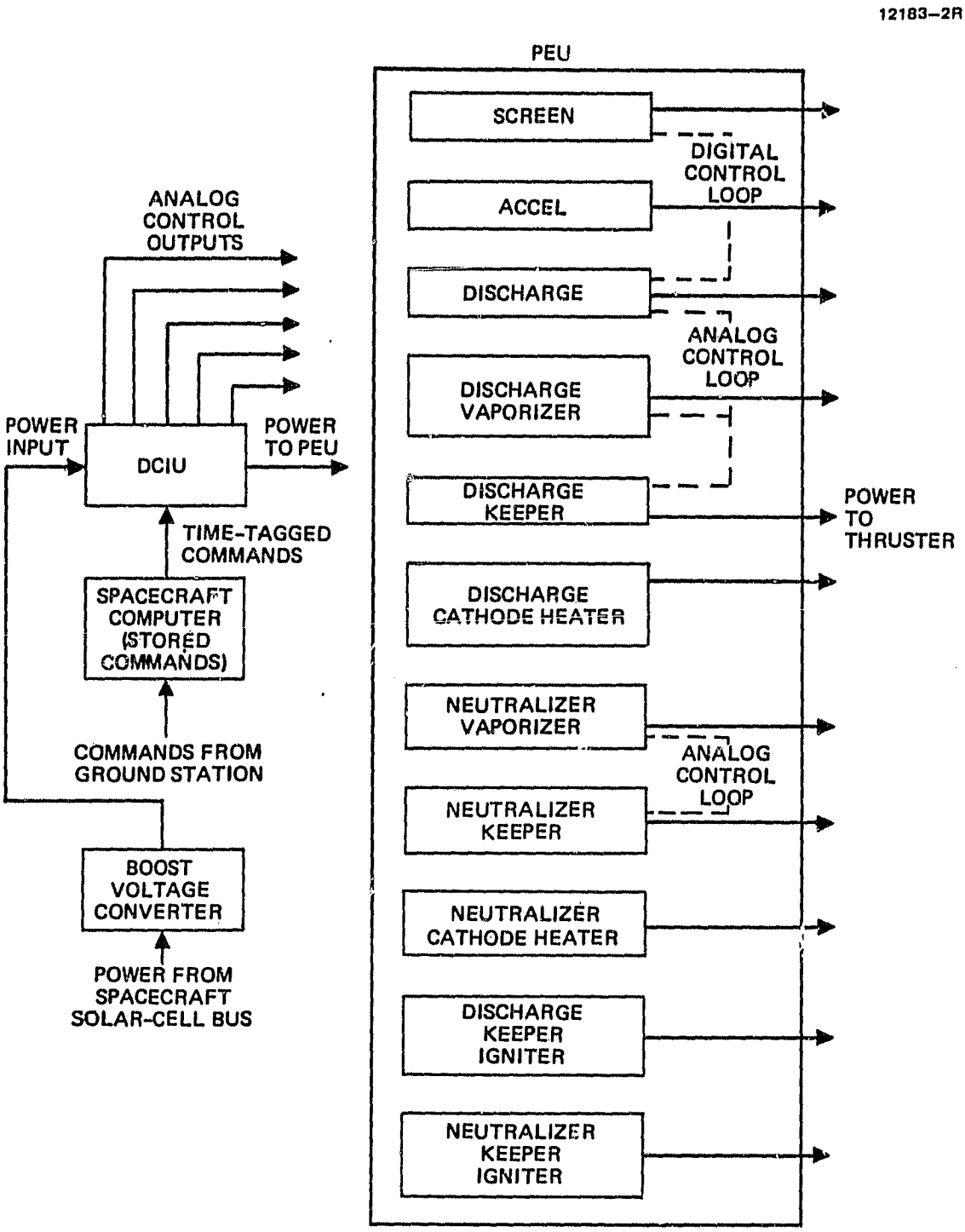

Figure 3(a). Functional relationship of DCIU, PEU, and TGBSU.

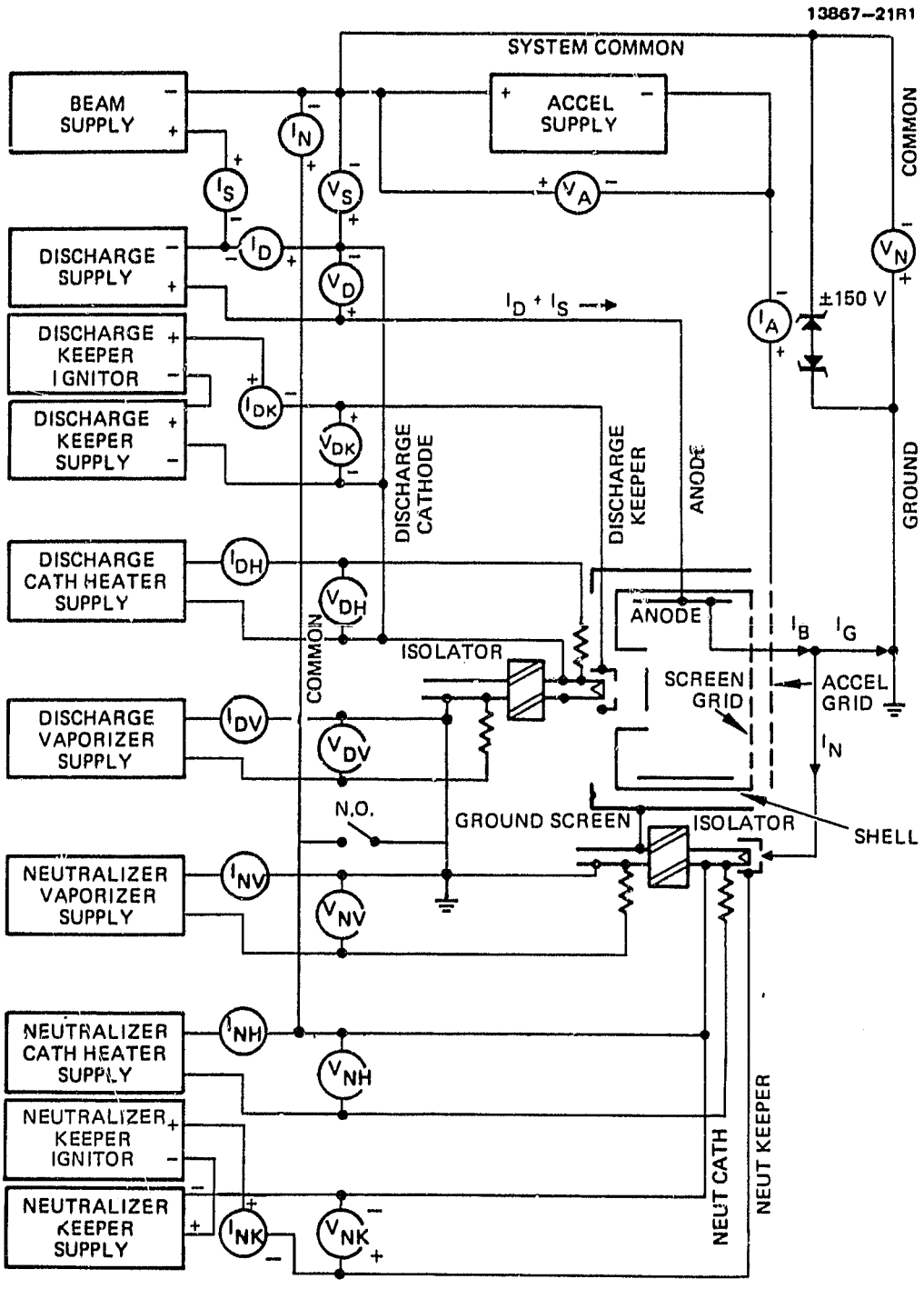

Figure 3(b). PEU-to-thruster wiring.

sequences of commands to the PEU to achieve the desired thrusting or non-thrusting condition. In addition, the DCIU possesses software provisions addressing a great depth of fault and failure conditions; this capability allows the thruster system to function automatically despite keeper extinctions, beam arcs, RTD (temperature-sensor) failures, etc.

The structure of the DCIU is shown schematically in Figure 4. The DCIU is based on a flight-qualified RCA 1802 CMOS microprocessor which executes algorithms that are stored in programmable read-only memory (PROM). Random-access (read-write) memory (RAM) is also provided; this memory is used to store ground-alterable setpoints, telemetry values, and as a system "scratchpad." DCIU commands take the form of 0-to-5-V analog voltages that are applied to the PEU control lines. These voltages are generated by a digital-to-analog convertor (DAC) and multiplexer (MUX). Similarly, telemetry data are acquired by an analog-to-digital convertor (ADC) and multiplexer; these data are written directly to RAM by a direct-memory-access controller (DMA). RAM data integrity is protected by a separate Hamming-code-based hardware device which can detect and correct single-bit RAM bitflips. This device scans memory frequently enough that the probability of two or more bitflips occurring in the same byte between scans is vanishingly small. DCIU operation will be described more fully in the section on DCIU software.

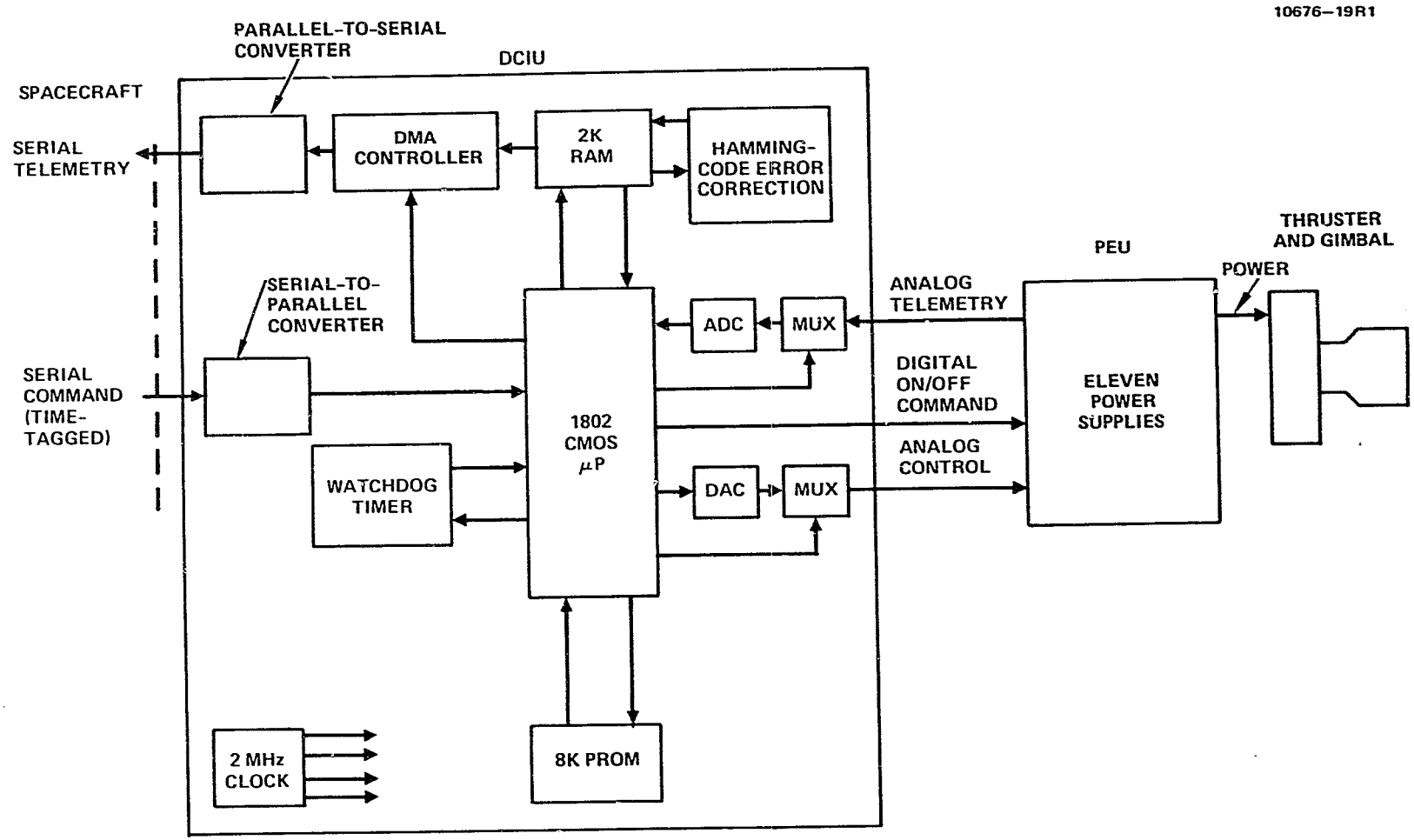

Figure 4. DCIU schematic diagram.

SECTION 3

EMT PERFORMANCE CHARACTERISTICS

In this section we describe performance characteristics of the EMT. We will include data which refer to both early EMTs having rolled-foil cathode inserts and to later EMTs having porous-tungsten cathode inserts. For reference, we will provide data obtained under contracts NAS3-21055 (IAPS flight contract) and NAS3-21741 (Ion Thruster System Cyclic Endurance Test) relating to flight-thruster performance and aging charcteristics.

Table 2 presents a summary of operation that is typical of EMTs in rolled-foil- and porous-tungsten-insert configurations, along with FMT performance characteristics. The performance differences between these three configurations are almost entirely attributable to the differences in cathode inserts. The rolled-foil inserts exhibited lower keeper voltages but somewhat irreproducible performance; this performance was highly sensitive to the details of the history of air exposures and cathode conditioning. This cathode-insert irreproducibility with rolled-foil inserts proved to be a principal cause of thruster-to-thruster performance variation (thruster dispersion). Porous-tungsten inserts, however, are comparatively insensitive to this history, but operate with somewhat higher keeper voltages (e.g., V_{DK}=13 V for porous tungsten, compared with V_{DK}=8 V for rolled foil), and with a new requirement for a small amount of cathode-heater power (P_{DH}≈2 W) during operation. The FMT data shown in Table 2 have been selected to be typical of operation that may be expected of the FMTs in space; higher-performance operation can be obtained from these thrusters, but at the expense of a narrower gap between the operating point and a region of thruster instability. This conservative choice of operating point has been made to assure maximum reliability when the thrusters are in fully automatic operation under DCIU control.

Table 2. 8-cm Thruster Performance

13867-27

PERFORMANCE PARAMETER \ THRUSTER TYPE AND CONFIGURATION	ENGINEERING-MODEL THRUSTER		FLIGHT-MODEL THRUSTER	FLIGHT CONFIGURATION THRUSTER
	ROLLED-FOIL CATHODE INSERT	POROUS-TUNGSTEN CATHODE INSERT	PERFORMANCE ON INITIAL OPERATION	PERFORMANCE AFTER EXTENDED OPERATION
THRUSTER SERIAL NO.	904	904R	908	903R
*THRUST F	5.11 mN	5.06 mN	5.11 mN	5.08 mN
*SPECIFIC IMPULSE I_{SP}	2723 s	2450	2547 s	†
TOTAL INPUT POWER P_T	116 W	122 W	124 W	130 W
*TOTAL EFFICIENCY η_T	0.588	0.500	0.514	†
*ELECTRICAL EFFICIENCY η_E	0.752	0.702	0.706	0.661
*THRUST-TO-POWER RATIO F/P_T	44.1 μN/W	41.5 μN/W	41.2 μN/W	39.0 μN/W
TOTAL PROPELLANT FLOWRATE I_{Hg}	92.1 mA EQUIV	101.3 mA EQUIV	98.8 mA EQUIV	†
*PROPELLANT UTILIZATION EFFICIENCY η_{Hg}	0.782	0.711	0.729	†
*DISCHARGE PROPELLANT UTILIZATION EFFICIENCY η'_{Hg}	0.844	0.756	0.768	†
*DISCHARGE SPECIFIC ENERGY ε_I	217 eV/ion	240 eV/ion	255 eV/ion	257 eV/ion
*BEAM CURRENT I_B	72 mA	72 mA	72 mA	72 mA
BEAM VOLTAGE V_B	1212 V	1187 V	1220 V	1196 V
ACCEL CURRENT I_A	270 μA	250 μA	222 μA	240 μA
ACCEL VOLTAGE V_A	-300 V	-297 V	-300 V	-289 V
KEEPER-TO-ANODE VOLTAGE V_δ	29.3 V	26.0 V	26.0 V	26.1 V
DISCHARGE VOLTAGE V_D	37.5 V	39.4 V	40.2 V	36.6 V
DISCHARGE CURRENT I_D	406 mA	419 mA	435 mA	485 mA
DISCHARGE KEEPER VOLTAGE V_{DK}	8.2 V	13.4 V	14.2 V	10.5 V
DISCHARGE KEEPER CURRENT I_{DK}	50 mA	60 mA	60 mA	75 mA
DISCHARGE CATHODE HEATER POWER P_{DH}	0	3.17 W	2.89 W	3.57 W
DISCHARGE PROPELLANT FLOWRATE I_{DHg}	85.3 mA EQUIV	95.4 mA EQUIV	93.8 mA EQUIV	†
NEUTRALIZER KEEPER VOLTAGE V_{NK}	15.7 V	16.0 V	16.2 V	15.3 V
NEUTRALIZER KEEPER CURRENT I_{NK}	497 mA	500 mA	500 mA	465 mA
NEUTRALIZER CATHODE HEATER POWER P_{NH}	0	5.16 W	3.82 W	4.86 W
NEUTRALIZER COUPLING VOLTAGE V_N	-12.0 V	-9.8 V	-12.4 V	-18.4 V
NEUTRALIZER PROPELLANT FLOWRATE I_{NHg}	6.8 mA EQUIV.	5.9 mA EQUIV.	5.0 mA EQUIV.	†

* QUANTITIES UNCORRECTED FOR BEAM DIVERGENCE AND DOUBLY CHARGED ION CONTENT OF THE BEAM

† UNKNOWN BECAUSE FLOWRATE CANNOT BE DIRECTLY MEASURED

Table 2 also presents data which reveal the changes in EMT performance characteristics that are associated with early cathode conditioning. The principal change that is evident is the reduction in keeper voltage and improved ease of ignition that occurs with time. Electrons enter the discharge chamber with an energy determined by the keeper-to-anode potential difference, $V_\delta = V_D - V_{DK}$. Therefore, reduced keeper voltage implies a lower discharge voltage, V_D, for the same value of V_δ. This reduced discharge voltage, V_D, results in both reduced discharge power, P_D, and reduced discharge-chamber sputter erosion.

SECTION 4

THRUSTER STABILITY AND CONTROL

In this section we describe the results of testing in three primary areas which are related to the general problem of assuring smooth and reproducible controllability of the thruster/power-processor combination. The most fundamental of these areas is the stability of thruster operation. By stability we refer to the absence of large-scale oscillations in any of the the thruster circuits that pass through plasmas; such oscillations can cause keeper extinctions, reduce performance, and endanger thruster or PEU [or "power processor"] integrity in a number of ways. The discharge current is the most sensitive current with respect to oscillations.

A second area of concern relates to the interaction between the thruster and PEU in a purely electrical sense; i.e., what electrical impedance does the thruster (as an electrical load) present to the PEU, and does this represent a stable and acceptable point on the load line of the PEU power supplies? Finally, the third area we describe concerns the problem of interface definition from the standpoint of control loops: what kinds of control loops (both analog and digital) are needed, and what phase/gain characteristics should they have?

A. DISCHARGE OSCILLATIONS

In testing of early EMTs, it was discovered that under certain operating conditions the discharge current became oscillatory, as illustrated in Figure 5, and restricted the thruster operating range, as shown in Figure 6. In the latter figure, note that the nominal operating point lies perilously close to the region of instability; this poses the hazard that a small perturbation during normal operation may result in instability.

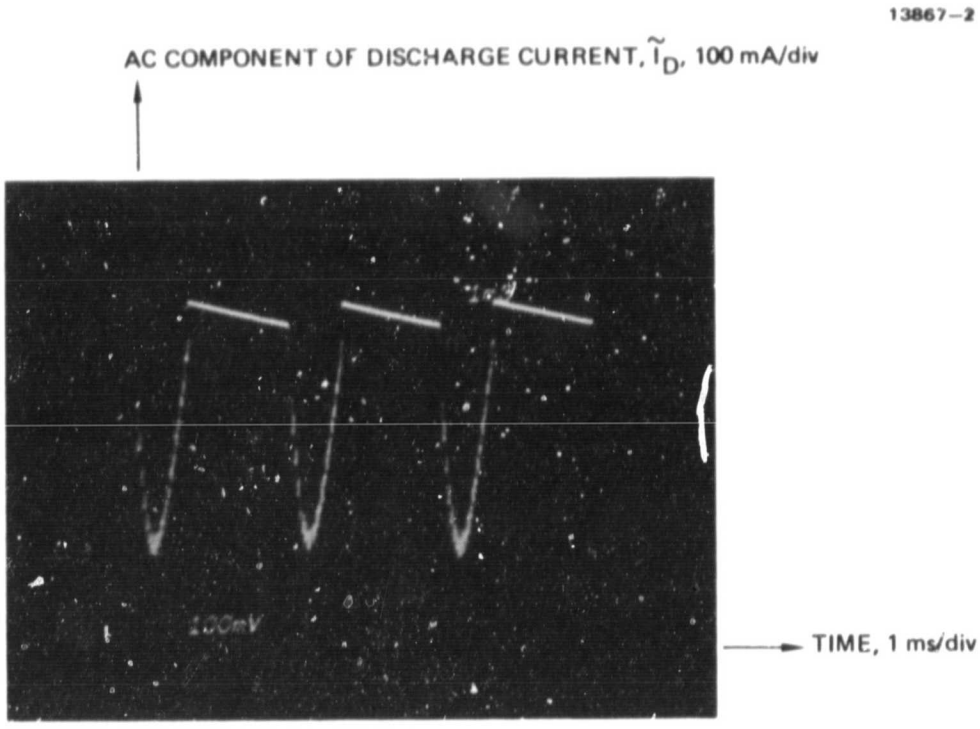

Figure 5. Discharge current oscillation in an early EMT.

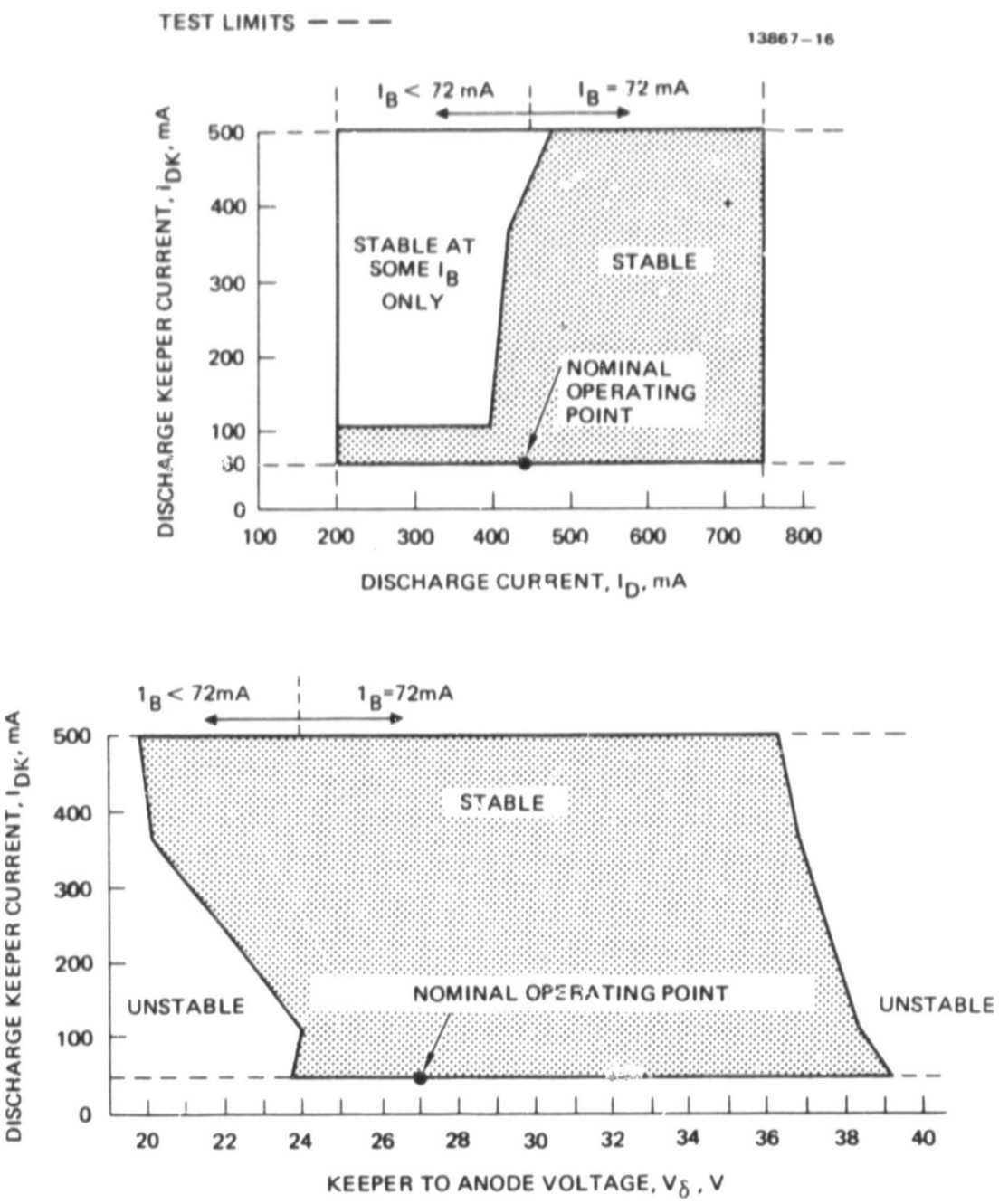

Figure 6. Stability diagram of EMT S/N 902 (data taken with laboratory power processor).

Discharge instability had not been observed in previous (laboratory-model) thrusters, and evidently corresponded to physical characteristics of the discharge chamber that were not reproduced accurately in the transition to the Engineering-Model design. (The Engineering Model design incorporated numerous design changes which were needed to accomodate the anticipated thermal- and launch-vibration environment, provide the required operational durability, and ensure that the dimensional tolerances would result in reproducible thruster performance.) This instability was sufficiently severe that the discharge current vanished completely except during large periodic surges of current; i.e., the thruster/power-processor behaved like a relaxation oscillator. Relaxation oscillations result in very poor propellant utilization (because un-ionized mercury is free to drift out of the discharge chamber during those periods when the discharge current is zero) and severe overloading of the accel power supply (because the large surges of discharge current produce beam current in excess of the beam-handling capacity of the extraction system). In addition to these difficulties, an oscillatory discharge current is associated with a high likelihood of keeper extinction. This is because discharge-current oscillation causes the discharge current to be completely off for many tens of milliseconds at a time, allowing the cathode to cool excessively.

The plasma inside the cathode polepiece (keeper plasma) is known to reside at a potential close to that of the keeper. Electrons migrate from the cathode polepiece volume into the main discharge by means of crossfield diffusion that is enhanced by collective plasma processes such as drift waves. These collective processes derive their motive force from the density- and potential gradients that reside within the keeper plasma and across the baffle gap. If electrons are injected into the keeper plasma in such a manner that the collective transport processes cannot function, then the impedance of the discharge rises above the potential supplied by the discharge power

supply, and the discharge current ceases. This process will repeat on a time scale commensurate with the sonic gas filling time of the discharge chamber, giving rise to a relaxation-type oscillation, usually in the 5 to 10 kHz frequency range. Two other classes of oscillations exist which have other characteristic frequencies: (1) thermal oscillations with frequencies in the 1-Hz frequency range, which corresponds to the thermal time constant of the cathode, and (2) normal collective plasma process oscillations, which produce MHz-band frequencies.

The foregoing discussion points to the importance of the details of density, temperature, and electric- and magnetic-field profiles in the interior of the cathode polepiece for maintaining the stability of the discharge.

B. ORIGINS OF DISCHARGE INSTABILITY

We undertook a substantial effort to uncover the origin of the discharge instability just described, and we found that two critical areas are involved: the thruster magnetic-circuit characteristics, and the discharge power-supply output impedance. We describe these two effects separately below.

1. Magnetic-Circuit Effects on Stability

Figure 7(a) and (b) gives a schematic depiction and an iron filing map of the EMT discharge-chamber magnetic circuit. Magnetic flux is generated by eight rod-shaped permanent magnets which are located outside the discharge chamber. Their magnetic flux is collected by the iron endplate and distributed by the cathode polepiece at the upstream end of the discharge chamber. At the downstream end, the flux is collected and distributed by the screen polepiece. A magnetic flux density of 0.5 to 5 mT is

13867-22

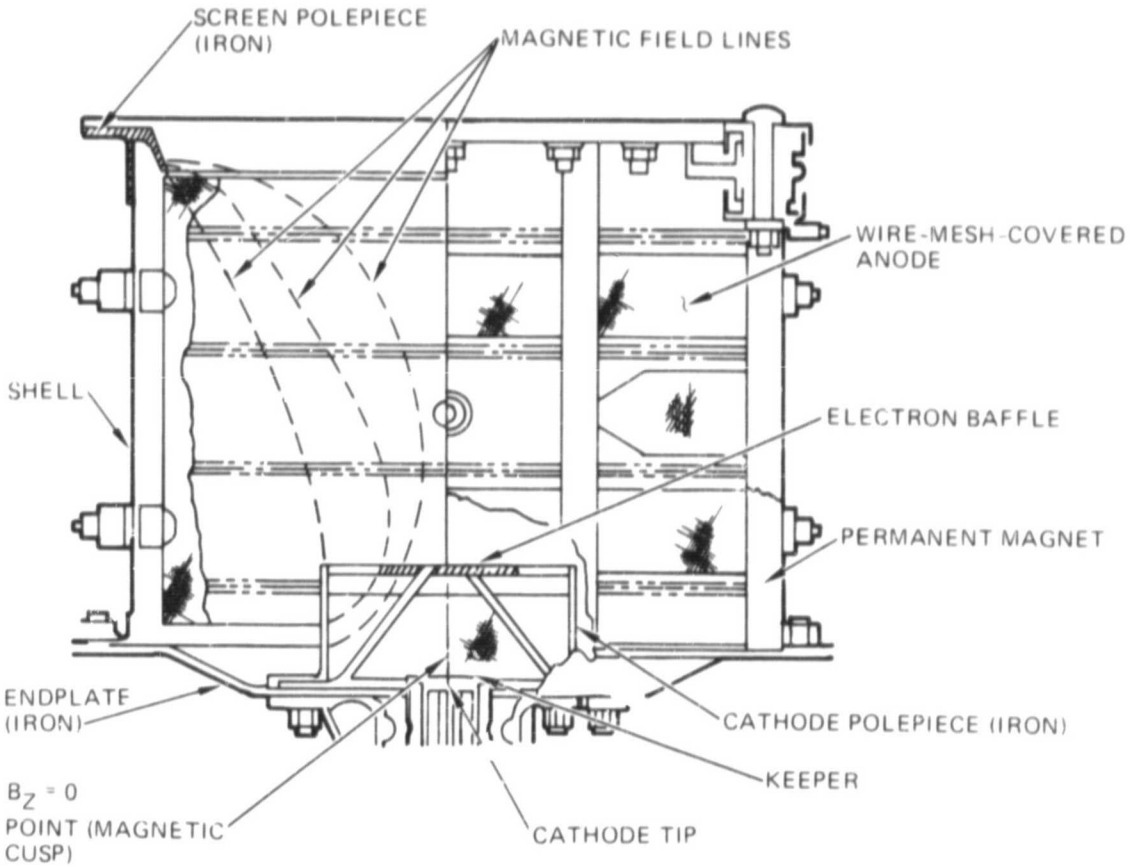

Figure 7(a). Discharge-chamber magnetic circuit.

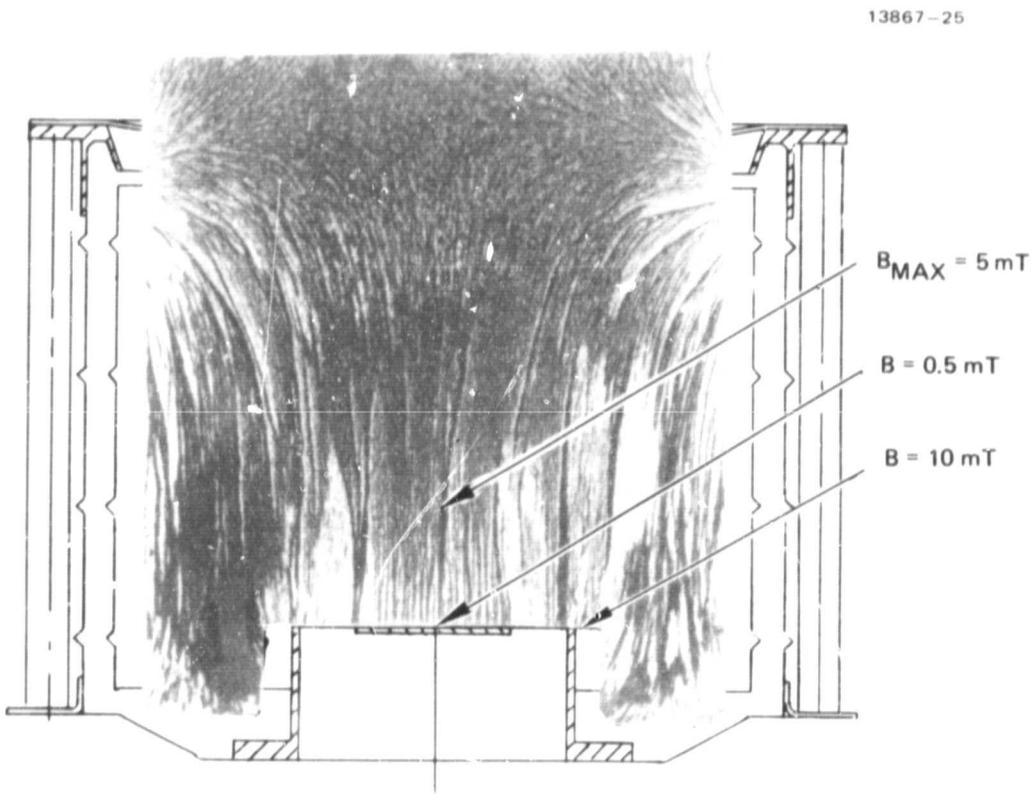

Figure 7(b). Discharge-chamber magnetic circuit: iron filing map.

produced throughout the discharge-chamber volume, as illustrated in Figure 7(a) and (b). The peak on-axis axial flux density of about 5 mT is located about 50 mm upstream of the screen electrode; the flux density exceeds 10 mT near the cathode polepiece tip.

In our investigations of the discharge-chamber magnetic circuit, we found that the following features were of critical importance to providing a broad range of stable operation:

- Sufficient magnetic permeability in the polepieces to avoid magnetic saturation.
- Placement of the cathode tip upstream of the zero of magnetic field that occurs near the thruster endplate.
- Magnetization of the permanent magnets so that they do not generate spurious field lines.

We discuss these topics separately below.

Magnetic Saturation

The first item listed above corresponds to the requirement to have sufficient thickness of permeable material so that magnetic flux is contained within the iron flux-conductors and polepieces. We found that the cathode polepiece in EMTs was insufficiently thick to assure absence of saturation. As shown in Figure 8, we recorded a hysteresis characteristic of the EMT magnetic circuit (we temporarily replaced the permanent magnets with electromagnets in order to make these measurements). Of particular note is the value of the magnetic field strength that corresponds to closure of the hysteresis diagram, i.e., to the condition that the B-H curve retraces the same path for both increasing or decreasing H. (Here B is the magnetic flux density and H is the magnetic field strength; they are given in SI units of Teslas and Amperes per meter, respectively.) This value of field strength corresponds to the condition that all

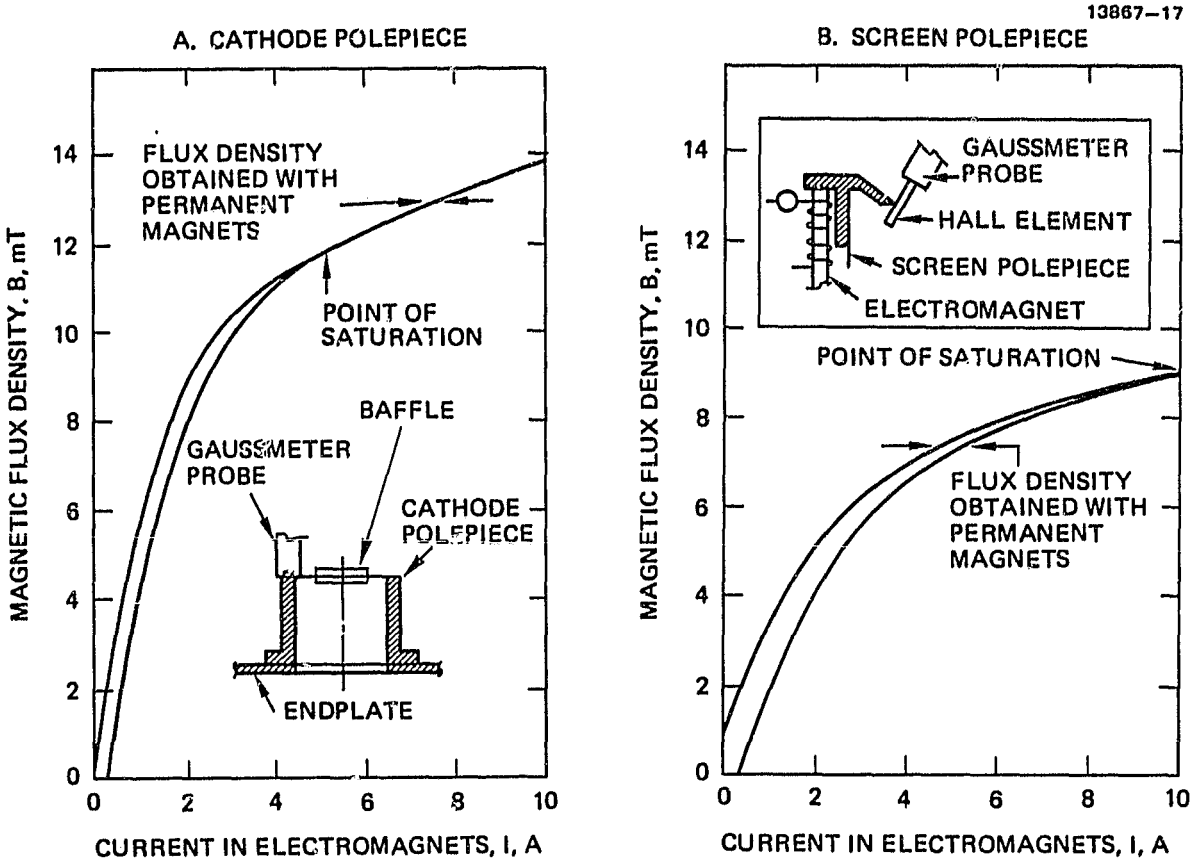

Figure 8. Saturation effects in the EMT magnetic circuit. The current I in the electromagnets is proportional to the magnetic field strength H.
(A) cathode polepiece;
(B) screen polepiece.

magnetic domains within the permeable material are aligned with the field. As seen in Figure 8, the flux density present in the cathode polepiece due to the permanent magnets is more than sufficient to cause saturation. In the screen polepiece, on the other hand, this is not the case.

Further increase of the field strength in the cathode polepiece above the saturation level will result in the field lines behaving as if no permeable material were present. In this case, magnetic-field lines leave the polepiece at some point corresponding with the details of saturation in the individual polepiece; in such a condition the field shape is determined in an important way by random effects within the polepiece. The result of this randomness is that the magnetic impedance across the baffle gap is variable and is not reproducible.

To eliminate this saturation problem, we revised the cathode polepiece design to incorporate a value of wall thickness equal to twice that of the original polepiece design. This substantially improved the range of stability of the test thruster. The design revision has been incorporated into the FMTs.

Cathode-Tip Location

A second factor that is of importance to thruster stability is the manner in which electrons are injected into the cathode polepiece volume by the cathode. The axial position of the cathode tip is important in this regard. In a previous contract (contract NAS3-18917) under which the 8-cm thruster was optimized, we discovered that the stability of the main discharge sensitively depended on the cathode tip position in the magnetic field and that discharge instabilities resulted if the cathode tip was placed downstream of the axial-magnetic-field zero (separatrix) which occurs near the plane of the endplate. Degraded, but stable performance was associated with a position too far upstream of the separatrix. Magnetic probing

of the EMT revealed that the axial position of this separatrix had shifted several millimeters downstream from the position that had been observed in the laboratory-model thruster. (See Figure 7(a).) This shift probably resulted from the different magnetic-material specifications and slightly different magnetic-circuit geometry that were used in the EMTs and FMTs. Tests indicated that thruster stability was insensitive to small magnetic perturbations in the region of the cathode tip in EM thrusters. This insensitivity may have resulted from the relative remoteness of the separatrix from the cathode tip, compared with the earlier laboratory-model thruster. These results lead to the conclusion that the cathode must be reproducibly positioned in the magnetic field, in order to avoid discharge instabilities.

Nondipole Magnets

In order to further determine the cause of discharge-current oscillations, we conducted extensive magnetic probing of EMT S/N 905. These measurements revealed azimuthal nonuniformities of the discharge-chamber magnetic field shape that proved to be caused by differences in magnetization among the eight magnets that ring the discharge chamber. In particular, several magnets exhibited iron-filing field maps that were strikingly nondipole in character. Figure 9(a) shows an iron-filing field map of such a magnet. Notice the filing pattern near the center of the magnet, which seems to suggest that field lines are emanating sideways from this region. We found that remagnetizing all of the magnets (with a magnetic field strength well in excess of that required to produce saturation of the alnico-V material) removed these suspect regions (see Figure 9(b)) and imparted a measurably higher azimuthal symmetry to the discharge-chamber field shape. The effect of this remagnetization was to increase the fraction of the EMT operating range that was stable.

13867-12

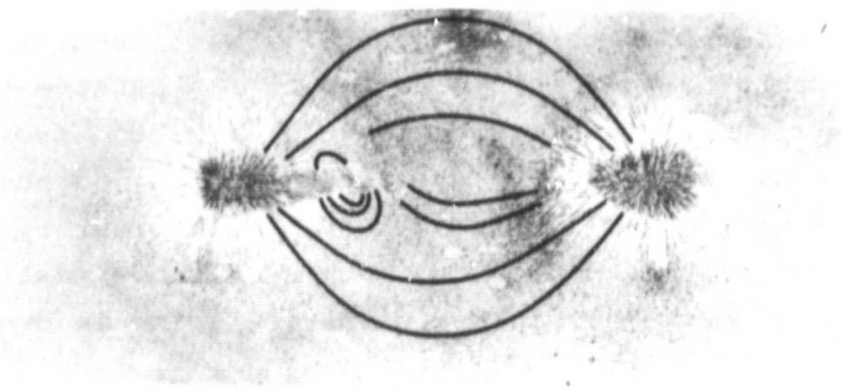

a. BEFORE REMAGNETIZATION

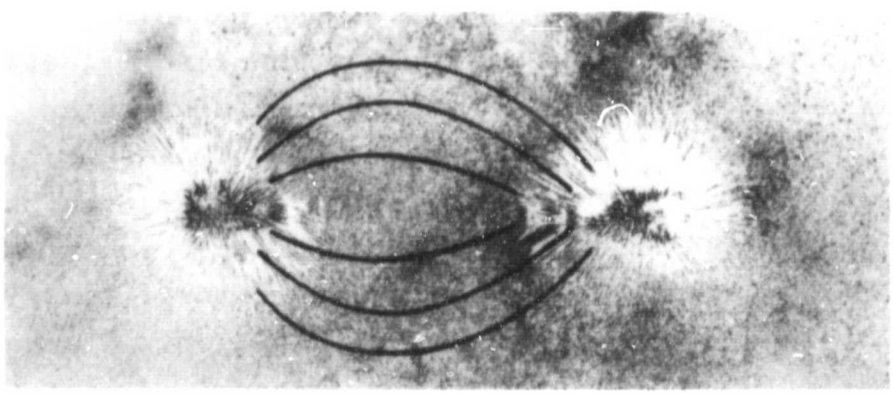

b. AFTER REMAGNETIZATION

Figure 9. Iron filing map of a thruster permanent magnet, exhibiting non-dipole region. (a) before remagnetization; (b) after remagnetization.

To summarize this discussion, we determined that the details of the thruster magnetic-circuit and field geometry substantially affect thruster operating stability. Figure 10 shows a before/after stability diagram which shows the effects of rectifying the thruster magnetic characteristics as discussed above. Other (non-magnetic) parameters which affect thruster operating stability are discussed in the next sections.

2. Power-Supply-Impedance Effects on Stability

The stability of the discharge is also strongly affected by the output-impedance characteristics of the discharge power supply. In general, flight-type power supplies of this kind have capacitive outputs, and the output capacitor is an energy reservoir which can participate in resonant mode-changing oscillations with the discharge. These oscillations are potentially damaging to the thruster, as we have described previously; they also pose a hazard to the power supply because large surge currents can be produced, and the noise of the oscillation can disrupt adjacent circuitry. In order to determine if these power-supply/discharge oscillations existed, we measured the frequency (phase-gain) response of the discharge/power-supply circuit. This type of measurement is desirable in that it provides an indication of the margin of stability that is present in the circuit; a narrow margin would raise concern that slight changes in discharge characteristics associated with aging or contamination could cause the system to become oscillatory. The phase-gain measurement does not reveal anything about the underlying physical processes which lead to oscillation, but it is a simple operational procedure for determining the presence of a potentially oscillatory region.

To make the phase-gain measurement, we added a small ac component to the output of the discharge power supply (by means of a signal generator), and we measured the resulting ac

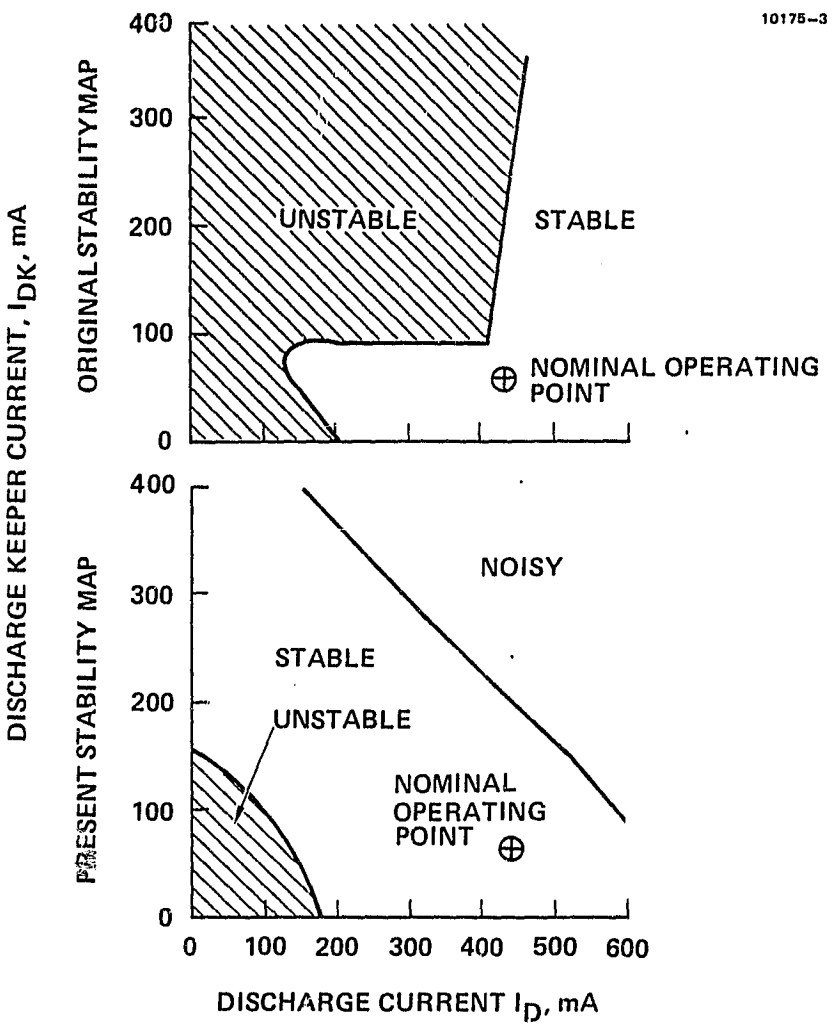

Figure 10. Thruster stability diagrams before and after magnetic-circuit revision and standardization.

component of the current while the thruster was in nominal full-beam operation. The impedance (voltage divided by current) is complex, because the current can be out of phase with the voltage. When the complex impedance was plotted as a Bode plot (i.e., phase angle and gain versus frequency), regions of potential oscillation could be readily identified; these are regions in which the gain is greater than unity (0 dB) and the phase angle is $\gtrsim 180°$.

We executed Bode plots for each of the critical power supplies (discharge, discharge keeper, and neutralizer keeper), and were able to establish power-supply output characteristics that provided adequate margins of stability. Some representative data are shown in Figure 11, where the gain and phase of the final (flight-configuration) neutralizer-keeper circuit are shown with the beam off, but with all other thruster parameters at their nominal operating levels.

C. VAPORIZER CONTROL LOOPS

The IAPS thruster subsystem is equipped with both digital and analog control loops which adjust the power to the discharge vaporizer to achieve the desired propellant flowrate. We consider the analog control loop in this section. Specifically, we will consider the choice of control parameter for the loop, and the loop gain that is necessary for best control characteristics. The majority of this section is concerned with the discharge-vaporizer control loop; a brief discussion of the neutralizer loop is given at the end of the section.

The traditional method of controlling the discharge vaporizer in small ion thrusters, having a single vaporizer supplying the entire discharge propellant flow, has been to sense the discharge voltage (cathode-to-anode potential difference) and apply more or less power to the discharge vaporizer to raise or lower the propellant flowrate, restoring

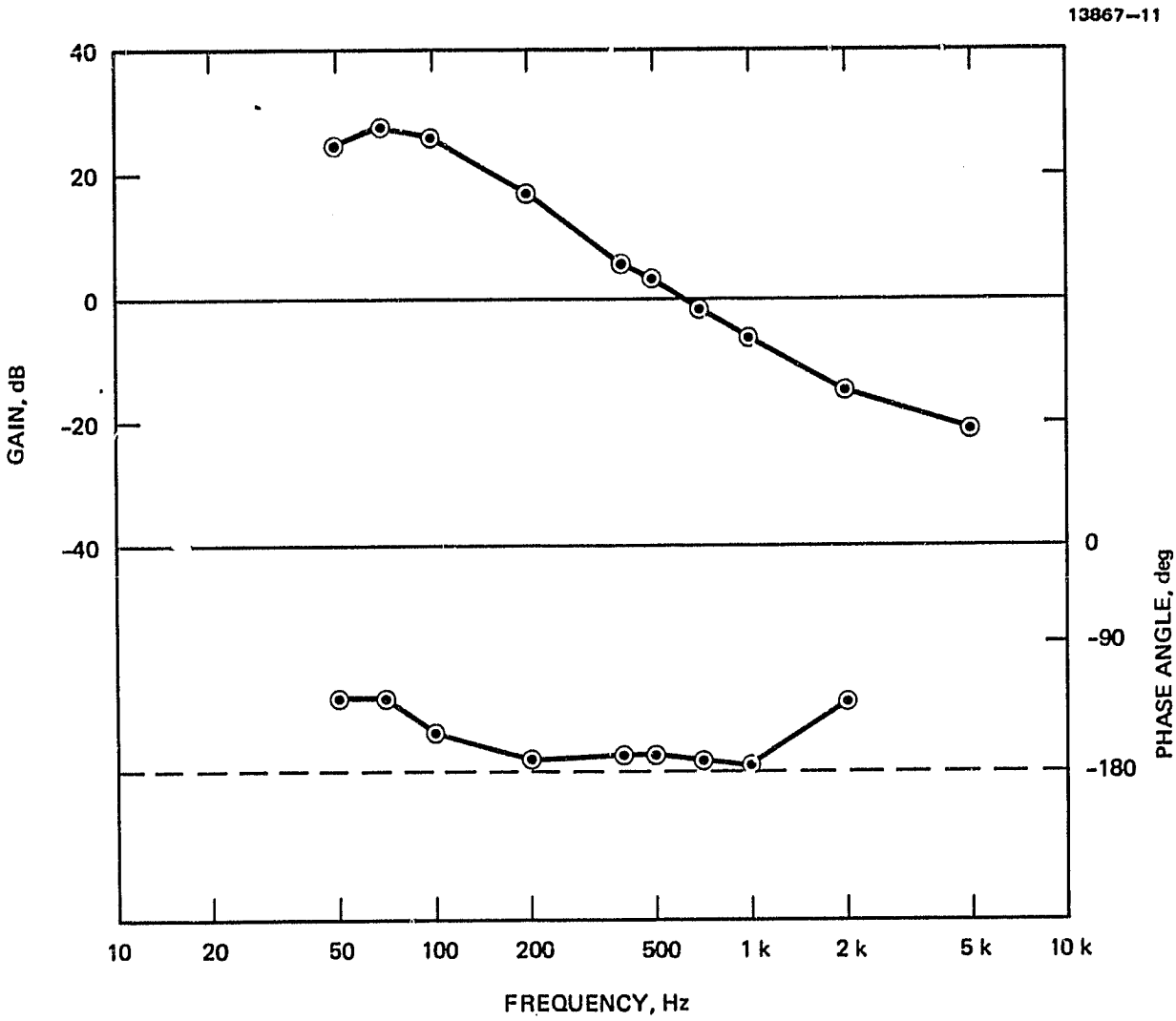

Figure 11. Bode plot of neutralizer-keeper circuit.

the discharge voltage to the desired value. Present evidence suggests, however, that the parameter that is most accurately correlated with thruster performance is the keeper-to-anode voltage V_δ, rather than the discharge voltage, V_D. This is because primary electrons, which produce the majority of ionization in the main discharge, originate at the potential of the plasma in the cathode polepiece (keeper plasma). This plasma has a potential close to that of the keeper (V_{DK}), so that primary electrons which fall into the anode-potential (V_D) discharge plasma have an energy which is derived from the potential difference $V_D-V_{DK}=V_\delta$. Any difference in control characteristics which would result from controlling on V_δ instead of V_D would necessarily appear subtle in laboratory testing, because the keeper voltage is relatively nonvarying; V_δ control would therefore appear to perform the same as V_D control, except for a setpoint offset determined by the keeper voltage. However, V_{DK} can change for a number of reasons (such as altered discharge current, cathode conditioning, and thruster aging), causing a shift from the desired operating point. To investigate the effects of keeper-voltage variability on vaporizer control-loop performance, we performed the following experiment: we recorded the discharge performance (in terms of propellant-utilization efficiency) by independently varying both the propellant flowrate and the cathode tip heater power, while adjusting the discharge current to maintain a constant beam current. Varying the cathode tip heat causes the keeper voltage to vary, simulating the effects of aging (or other effects which would change V_{DK}), while adjusting discharge current to maintain constant beam current mimics the action of a digital control loop that is implemented in the DCIU. In Figures 12 and 13 we plot the results of these measurements in two ways: in Figure 12 the data are plotted against V_D, and in Figure 13 the same data are plotted against V_δ. Notice that the parametric importance of the cathode tip

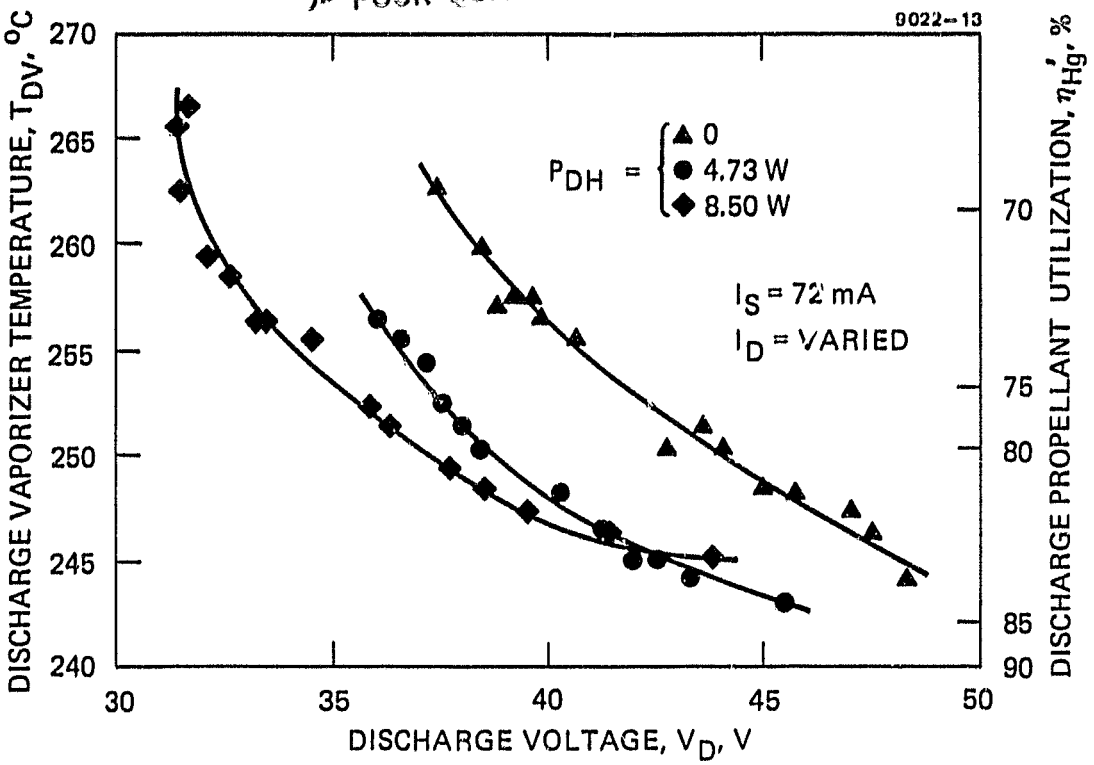

Figure 12. Thruster performance as a function of discharge voltage.

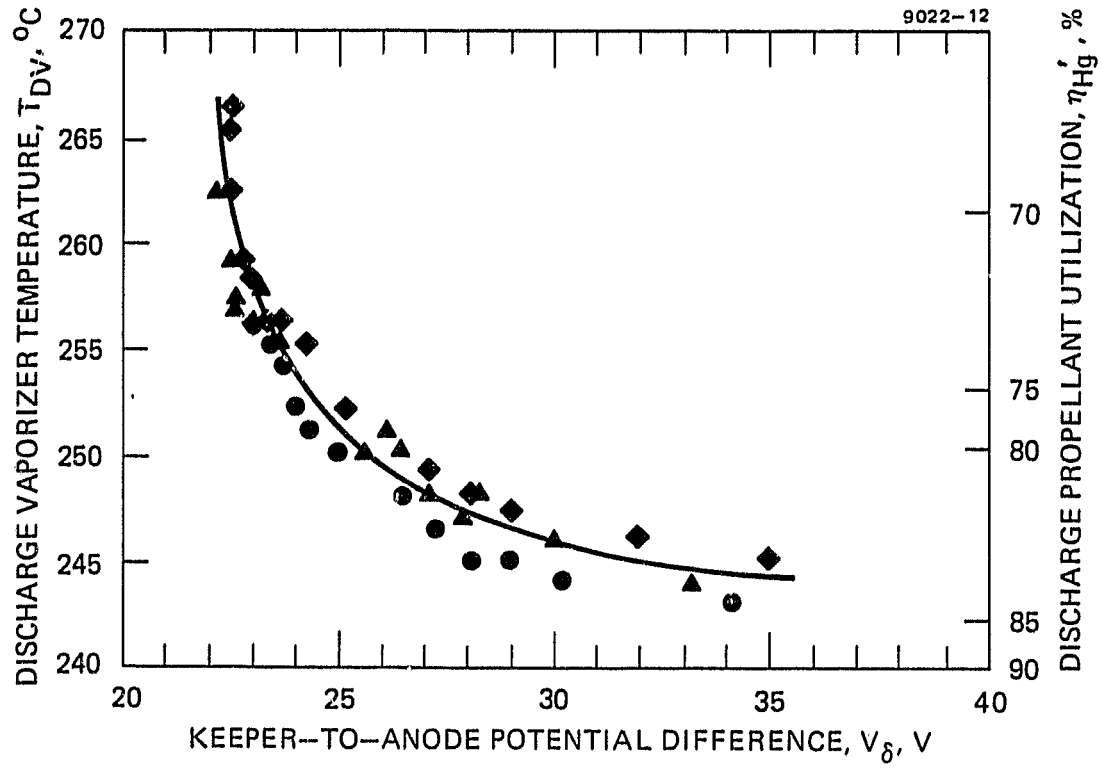

Figure 13. Thruster performance as a function of keeper-to-anode-voltage.

heat vanishes when V_δ is used as the independent variable. These data validate the choice of V_δ as the control parameter for the analog discharge-vaporizer control loop. The value of V_δ = 26.5 V in Figure 13 provides the best tradeoff between propellant utilization efficiency and discharge specific energy.

Figure 14 shows the discharge-vaporizer control loop in schematic form. This loop is characterized by the transter functions of both physical elements (e.g., the $V_\delta(I_{DHg})$ correspondence) and circuit components (e.g., the operational amplifiers), so the overall loop transfer function is knowable only in an empirical sense. To determine the optimum gain setting for the loop (i.e., value of the operational-amplifier feedback resistors), we configured a thruster and PEU with adjustable feedback, and manually increased the gain until oscillation occurred. After reducing the gain slightly from this point, we recorded a Bode plot (phase-gain characteristic) of the overall control loop. We then repeated this procedure until an acceptable balance between loop response and phase margin was achieved. Figure 15 shows the results of these measurements. The actual loop gain employed in the IAPS flight system differs somewhat from that shown in Figure 15 because of a change in loop characteristics that may be attributed to a revised cathode-insert design (see Section 6).

Figure 16 shows a Bode plot of the Neutralizer control loop following an optimization procedure similar to that described above (except that the neutralizer keeper voltage is used as the control parameter). The strong nonlinearity of the characteristic shown in Figure 16 is indicative of the complex physical processes involved.

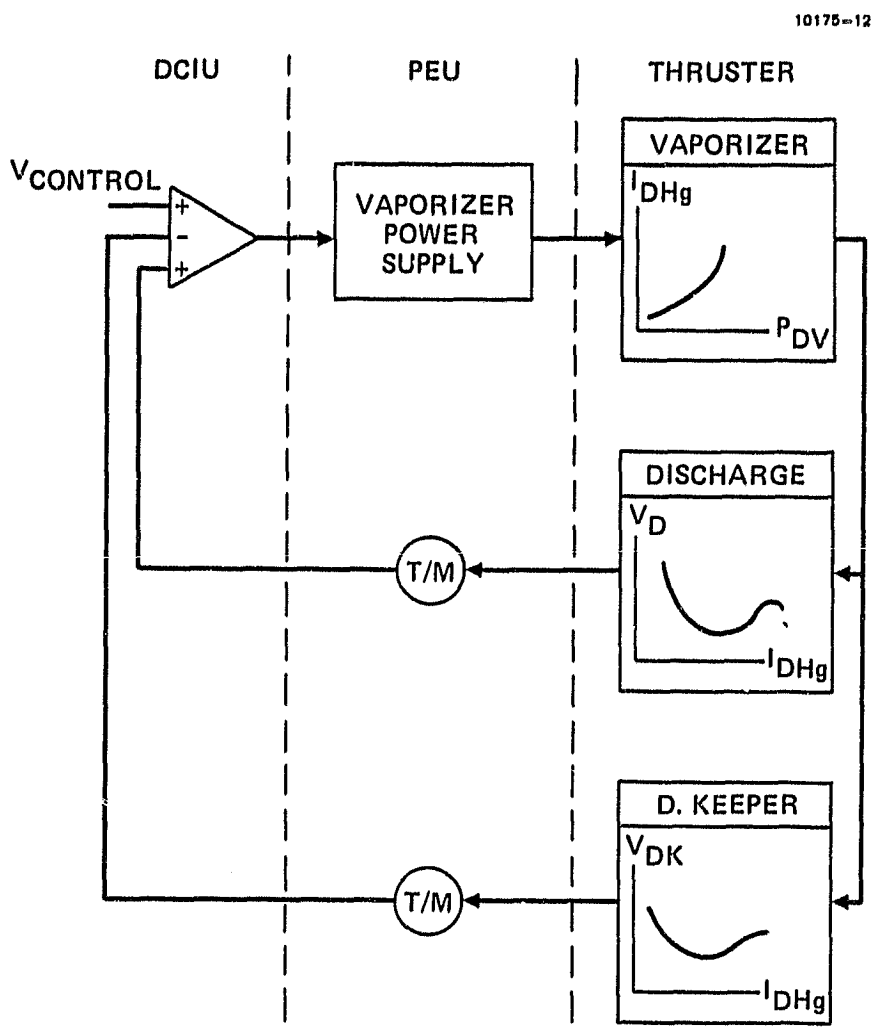

Figure 14. Schematic of discharge-vaporizer control loop.

10175-7

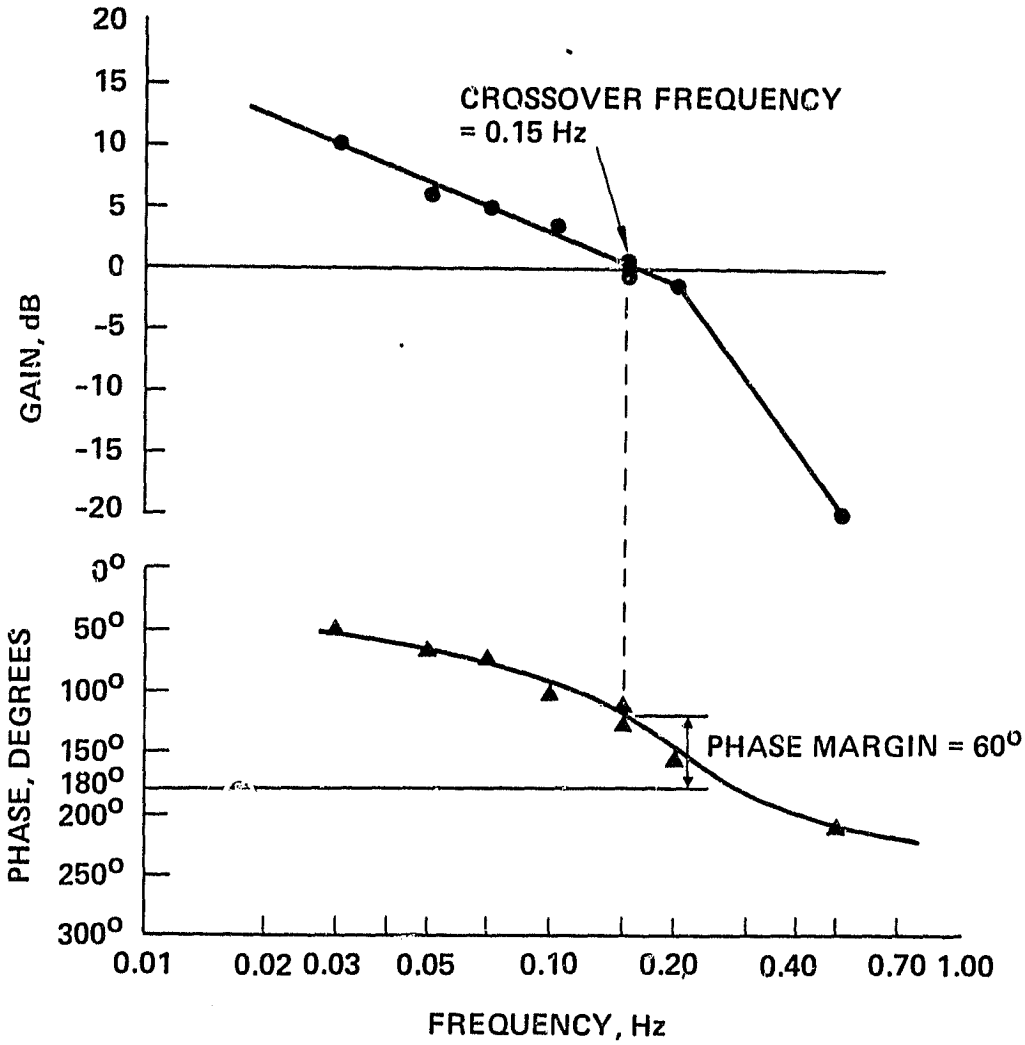

Figure 15. Bode plot of discharge-vaporizer control loop (corresponding to optimized parameters).

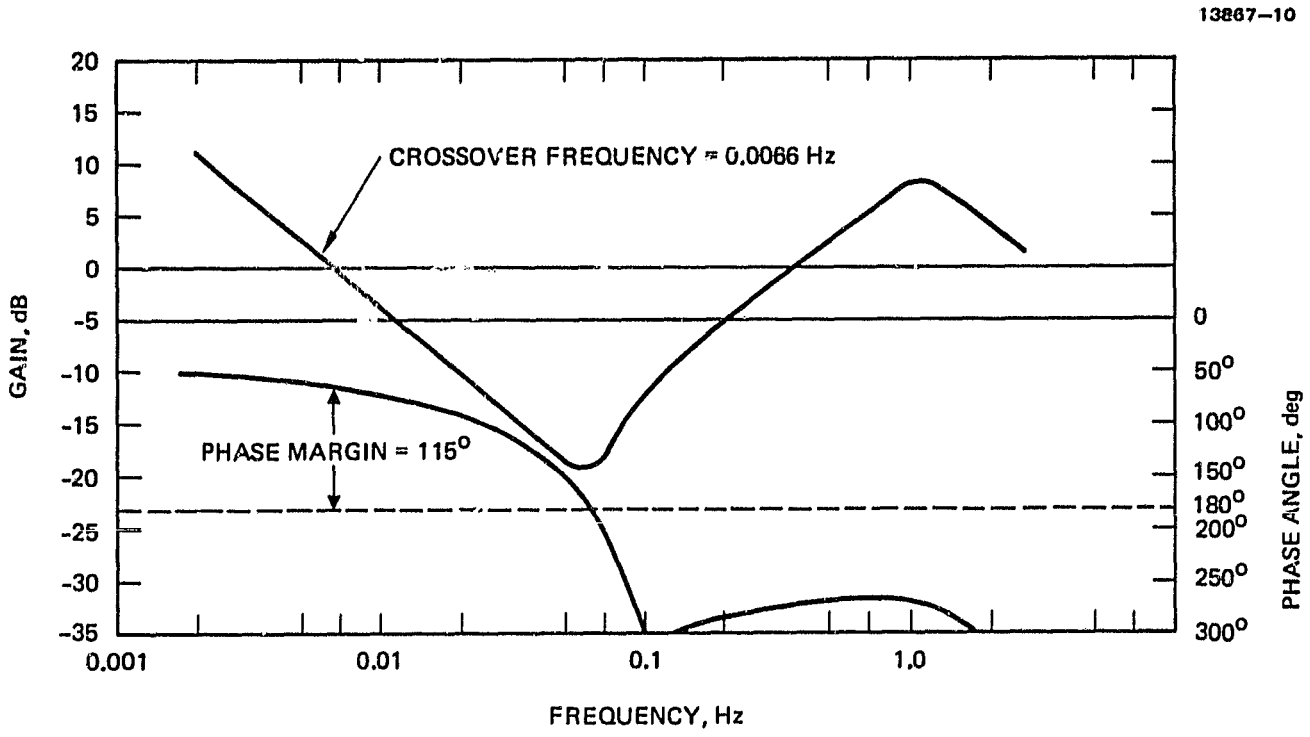

Figure 16. Neutralizer-vaporizer control loop Bode plot.

SECTION 5

THRUSTER CONTROL ALGORITHMS

Because the IAPS mission will be conducted in low Earth orbit (LEO), telemetry access to the spacecraft will be of limited duration, and there will be very limited capability for real-time interaction with the IAPS thrusters. Accordingly, the DCIU has been designed with the capability to operate the TGBSU with an exceedingly high degree of independence from the ground. The software to accomplish this task encompasses routines which not only take the thruster between any of a number of defined operating modes, but also automatically restore normal operation following fault occurrences, and automatically implement workarounds for a large number of single-point hardware failures. Still other failures can be handled by ground-enabled failure-recovery mechanisms. Finally, the most critical of the reference setpoints used by the software can be altered by ground command to accomodate changes in thruster characteristics which may arise from aging, contamination, unanticipated thermal conditions, etc. To provide support of the IAPS Flight-program software-development effort, portions of the present contract were directed toward testing and characterization of the TGBSU/software interaction. In the course of this effort, we helped to define:

1. Algorithms for routine thruster operation;
2. Setpoint allocations for hardware implementation in the DCIU;
3. Reference-level data for inclusion in DCIU software;
4. DCIU timeouts for thruster transitions; and
5. Recovery algorithms such as cathode hardstarting.

We also participated in testing in which the response of the thruster to automatic DCIU control (using the algorithms mentioned above) was evaluated and the algorithms were optimized.

While it would be unreasonable to describe all of the above activities in detail here, we will give a brief background concerning the control philosophy and DCIU software design, and we will describe a specific example of the development of a normal-fault workaround.

CONTROL PHILOSOPHY AND SOFTWARE OVERVIEW

Figure 17 shows a functional diagram of the DCIU software. The bottom of the diagram, labeled "application routines", corresponds to thruster control activities. These small-scale activities are portions of transitions between the thruster operating modes. A "mode manager" is aware of present mode and destination mode, and it calls appropriate transition tasks (in sequence, if necessary) to arrive at the destination mode. Routines to recover from faults such as keeper extinctions, which occur during mode transitions, are called by the transition tasks. In addition, the "antiflood" routine is called as a normal procedure, because thruster flooding is a "fault" which normally occurs during the ignition process. The same recovery routines are called by the "thruster monitor" routine if a fault occurs when the thruster is in a stable mode. The thruster monitor also adjusts discharge current to maintain a constant level of beam current.

The multitasking capability that is implicit in Figure 17 is accomplished by an interrupt scheme in which the microprocessor sequentially services each active task. The "executive" routine contains provisions to identify which tasks are active (task-table maintenance), as well as perform input/output-handling and other housekeeping activities.

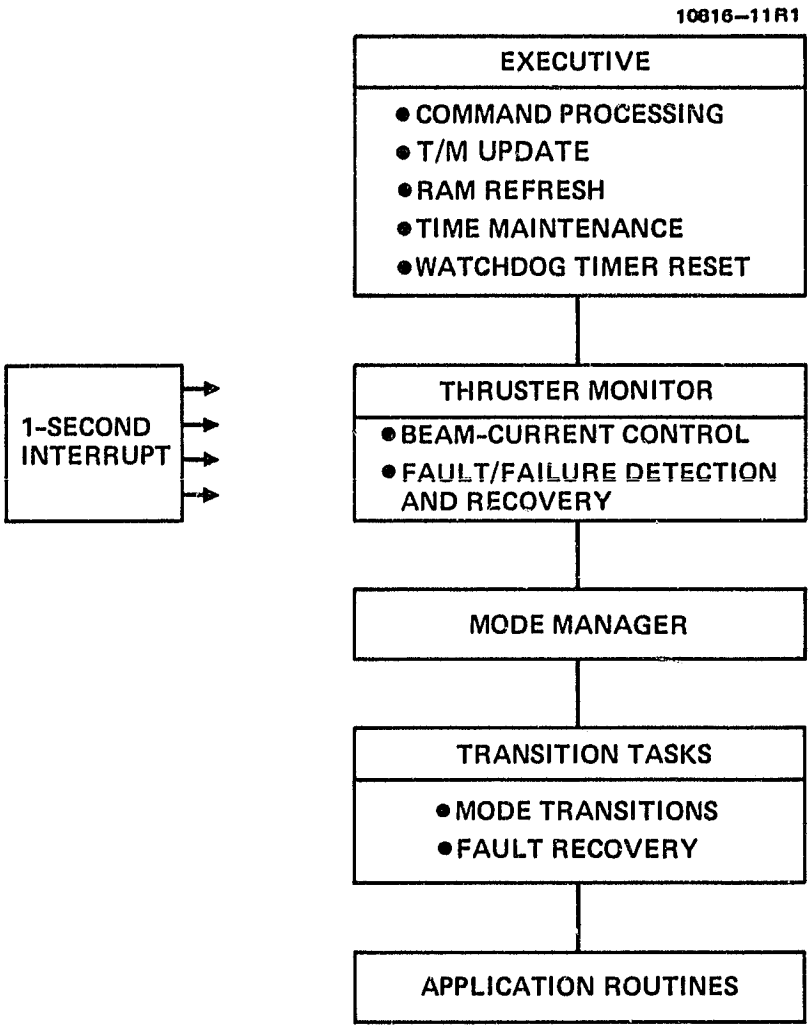

Figure 17. Block diagram illustrating DCIU software hierachy.

Figure 18 illustrates the thruster operating modes and allowable transitions in a state diagram, and Table 3 explains the functions and characteristics of the modes. Each of the eleven modes is accessible along paths indicated by the arrows by a single ground command. Also, compound transitions to BF or BR are allowed on a single command. Failure to reach the mode within a prescribed time (or for any of a number of other reasons) causes a transition to the "OFF" mode or a maintenance mode.

Figure 19 is a block diagram of the off-to-full-beam transition, passing through the steady-state-standby mode. The sequence represented in this figure is the result of extensive testing; it provides reliable transitions under extreme thermal conditions and under a wide variety of fault/failure conditions. One such normal condition is flooding of the main discharge. This is automatically corrected by the "ANTIFLOOD" routine described below.

Figure 20 is a highly simplified flow diagram of the thruster monitor. As can be seen from this figure, the monitor repetitively checks to see that thruster operation is within the prescribed bounds of its current mode, and calls recovery routines if corrective action is required. Another function performed by the Monitor is the adjustment of the discharge current to maintain the desired beam current. This adjustment is carried out every 10 s.

Table 4 is a partial listing of fault- and failure-recovery routines contained within the DCIU programming. The antiflooding routines are one type of these fault-recovery routines. Antiflooding is invoked when the DCIU perceives that the closed-loop vaporizer operation is controlling on a false control point, as illustrated in Figure 21. "Flooding" of the discharge can occur if the analog control loop described earlier is engaged when the control voltage, V_δ, is higher than the setpoint with the vaporizer temperature above the nominal operating level.

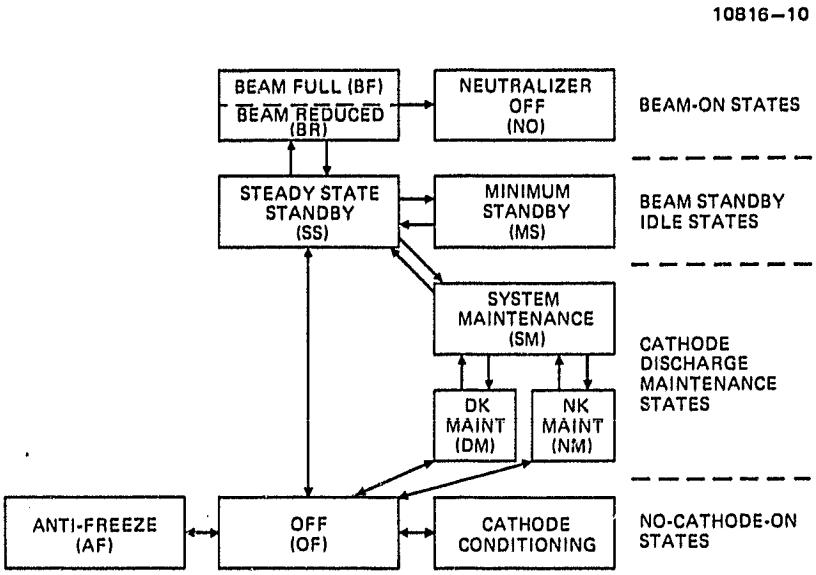

Figure 18. Block diagram of IAPS thruster operating modes and transitions.

Table 3. Steady State Operating Modes Programmed in Thruster Subsystem Controller

NO.	MODE	DK ON?	NK ON?	DIS. ON?	BEAM ON?	SPECIAL CONDITIONS	PURPOSE
0	Off	N	N	N	N	No Supplies On	-------
1	Antifreeze	N	N	N	N	DV and/or NV on low	Prevent Mercury Freezing
2	Conditioning	N	N	N	N	DH and/or NH On	Cathode Conditioning
3	Discharge Cathode Maintenance	Y	N	N	N	Low Flow and Power	Avoid Ignition Problems
4	Neutralizer Maintenance	N	Y	N	N	Low Flow and Power	Avoid Ignition Problems
5	System Maintenance	Y	Y	N	N	Low Flow and Power	Avoid Ignition Problems. Idle Condition
6	Steady State Standby	Y	Y	Y	N	----------	Idle Condition. Fast Beam Acquisition.
7	Minimum Standby	Y	Y	Y	N	Low Flow and Power	Idle Condition
8a	Full Thrust	Y	Y	Y	Y	Nominal Operation	Nominal 5.07 mN (1.14 mlb) Thrust
8b	Reduced Thrust	Y	Y	Y	Y	Minimum Power Thrusting	Reduced 4.45 mN (1.00 mlb) Thrust
9	Neutralizer Off	Y	N	Y	Y	Neutralizer Turnoff with Beam On	Experimental. Beam Neutralization Investigation

SYMBOLS: DV - discharge vaporizer; NV - neutralizer vaporizer; DH - discharge cathode tip heater; NH - neutralizer tip heater; DK - discharge cathode keeper (ignited); NK - neutralizer keeper (ignited); and DIS - main discharge.

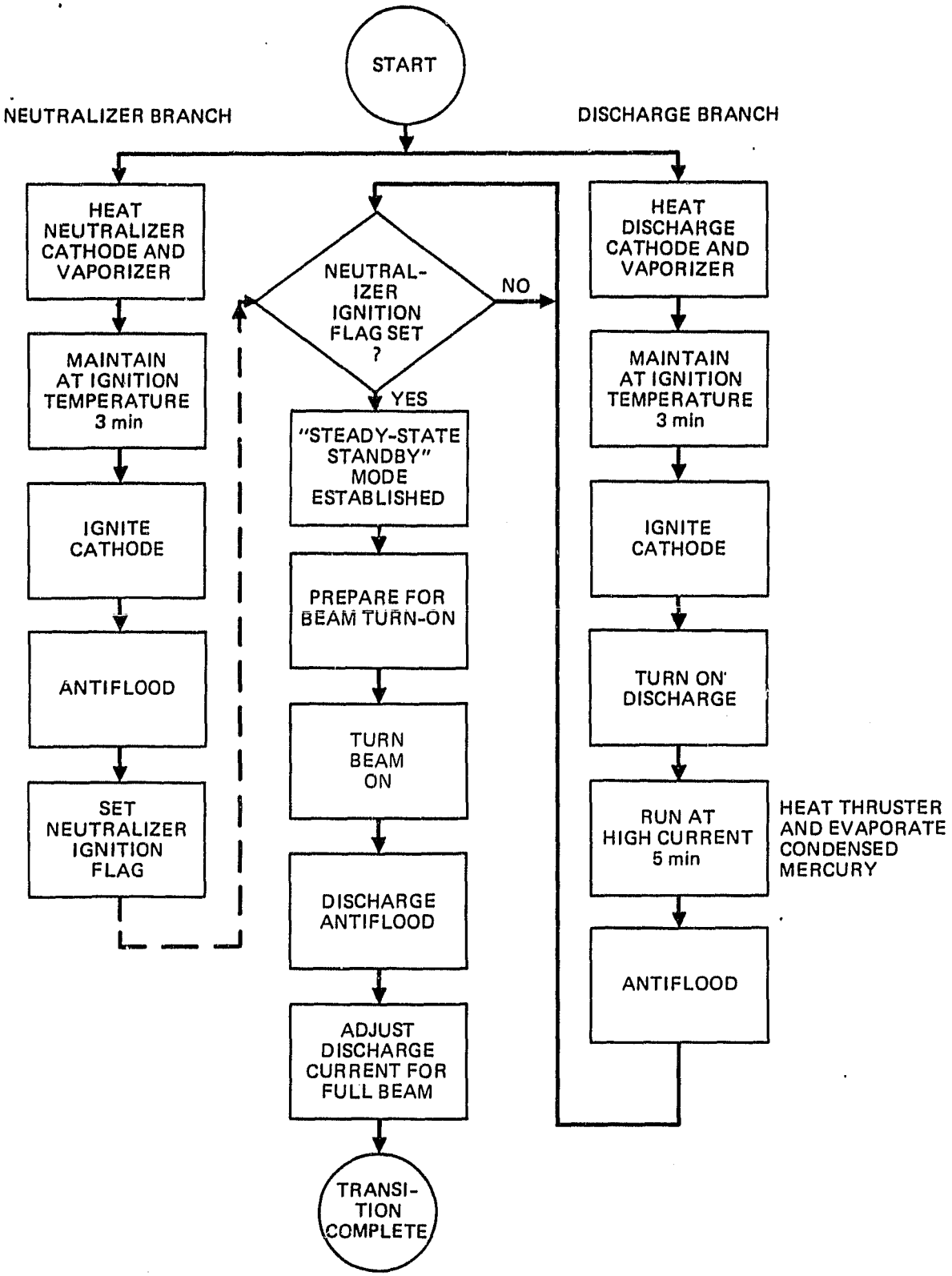

Figure 19. OFF to BEAM FULL mode transition.

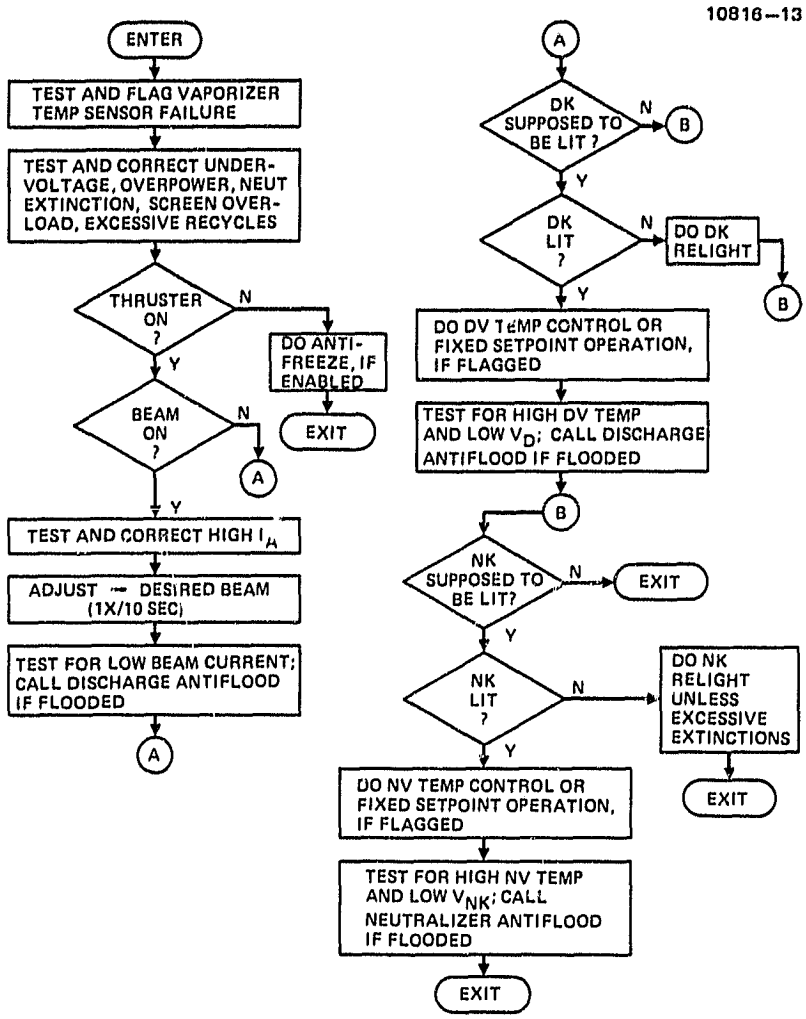

Figure 20. Flowchart of thruster monitor (executed once per second).

Table 4. Thruster Subsystem Faults and Failures Addressed by DCIU Software

FAULT/FAILURE	RECOVERY ACTION
Discharge vaporizer temperature sensor failure.	Time-based or fixed vaporizer setpont workarounds, incorporated in all algorithms requiring sensor information, automatically invoked.
Neutralizer vaporizer temperature sensor failure.	Same as above.
Discharge cathode hardstart.	Extensive hardstart algorithm automatically invoked. May be locked out by ground command.
Neutralizer hardstart.	Same as for discharge cathode hardstart.
Discharge cathode extinction.	Relight sequence automatically initiated. Mode recovery after relight.
Neutralizer extinction.	Relight sequence automatically initiated. Mode recovery after relight.
Discharge flooding.	Anti-flooding routine automatically called and executed until condition corrected.
Neutralizer flooding.	Same as for discharge flooding.
Grid short or high accelerator drain current.	High voltage recycle sequence automatically initiated.
Excessive high voltage recycling (> 64 recycles/hr.)	Thruster shutdown automatically executed. Ground command required for restart.
Power electronics unit power consumption > 200 W	High voltage automatically removed and recovery algorithm executed.
Power electronics unit bus voltage < 50 V	Shutdown automatically executed. Ground-commanded re-initialization and restart required.

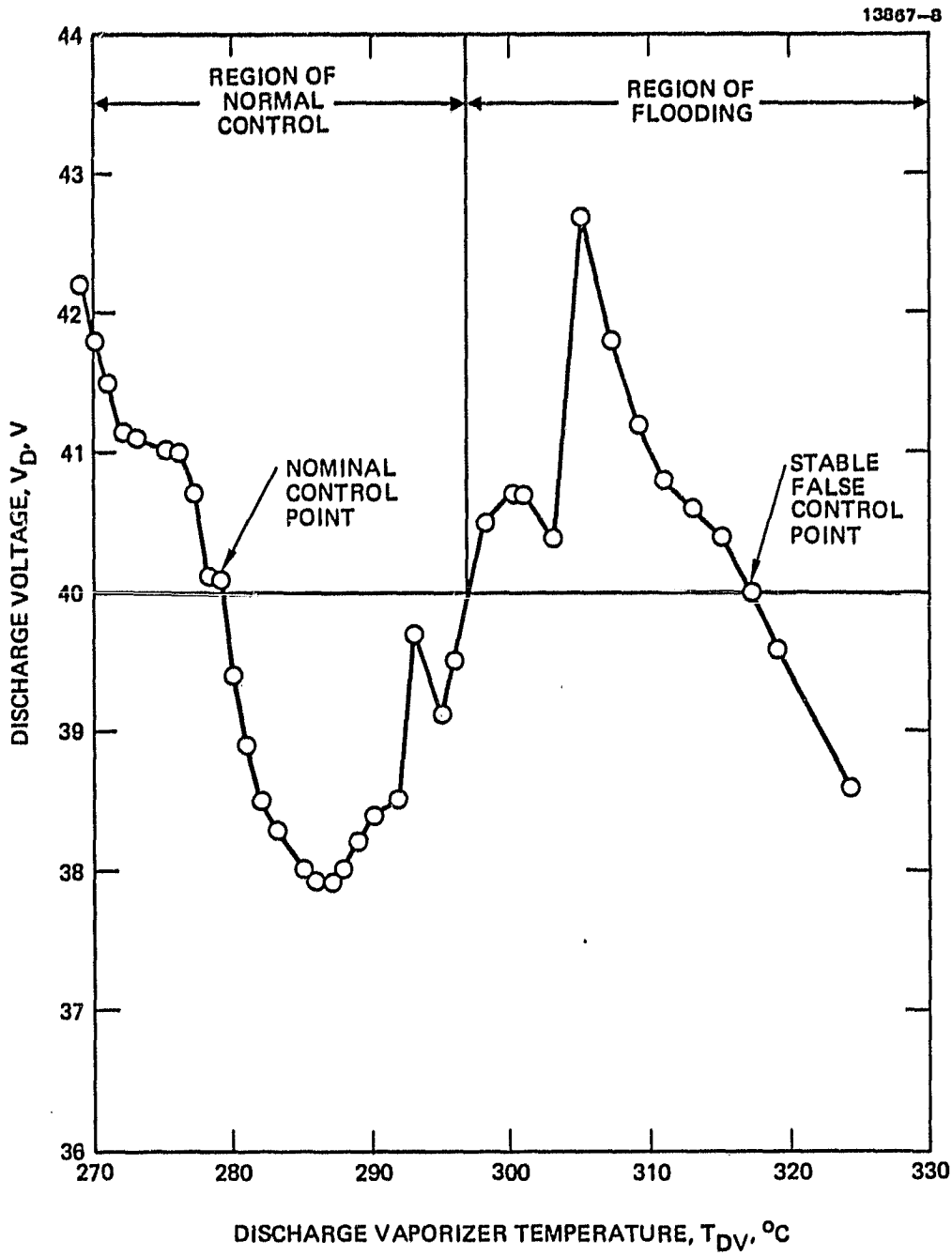

Figure 21. Discharge-vaporizer control curve, illustrating false control point (flight thruster S/N 908).

In this case, the loop increases the vaporizer temperature until the thruster reaches a false control point.

Figure 21 illustrates the flooding process. When the vaporizer temperature falls within the "region of normal control", the action of the analog loop will be to drive the system to stable operation at the nominal control point. However, if the loop is closed when T_{DV} falls within the region labeled "region of flooding", then it will drive the system to stable operation at the false control point indicated on the figure.

ANTIFLOOD, when called (a number of indicators will trigger a call to ANTIFLOOD), reduces the vaporizer power and tracks the control voltage until three criteria have been satisfied: (1) the vaporizer temperature is below a maximum level set just below the maximum vaporizer temperature of the region of normal control, (2) the time rate of change of the voltage is positive, and (3) the voltage has risen a specified amount over the minimum voltage reached. At this time ANTIFLOOD closes the analog loop to adjust operation to the correct control point. It can be seen from Figure 21 that this stratagem will reliably achieve operation at the correct control point.

SECTION 6

CATHODE CHARACTERIZATION

In early testing of the 8-cm EMT, it was discovered that the original cathodes, which were based on rolled-tantalum-foil (RTF) cathode inserts, were exhibiting irreproducible behavior. While the performance of these cathodes was outstanding, the repeated air exposures and reconditioning procedures that normally attend laboratory development testing tended to degrade performance. In particular, both the ignition requirements of the rolled-foil cathodes (open-circuit keeper voltage and preignition cathode-heater power) and their steady-state operating characteristics (keeper voltage) varied substantially from one test to the next, and from one cathode to the next. Our data base of test results with these inserts was insufficient to assure that flight thrusters would not exhibit the same type of dispersion, even though they would be subjected to more cautious environmental control than earlier laboratory- and engineering-model thrusters. Hence it was decided to reconfigure the FMT design by incorporation of the more rugged porous-tungsten (PW) inserts in the cathodes.

In this section we describe the characteristics of PW inserts and the work we conducted to develop an acceptable PW cathode insert and integrate this new design into the 8-cm thruster.

A. POROUS-TUNGSTEN INSERT CHARACTERISTICS AND FABRICATION

Figure 22 illustrates the PW cathode insert as used in the FMTs. The insert consists of a hollow cylinder of sintered porous tungsten which is impregnated with a barium-calcium-aluminum oxide ($BaO:CaO:Al_2O_3$ in a 4:1:1 molar ratio) emissive material. The upstream end of the insert is fitted with a

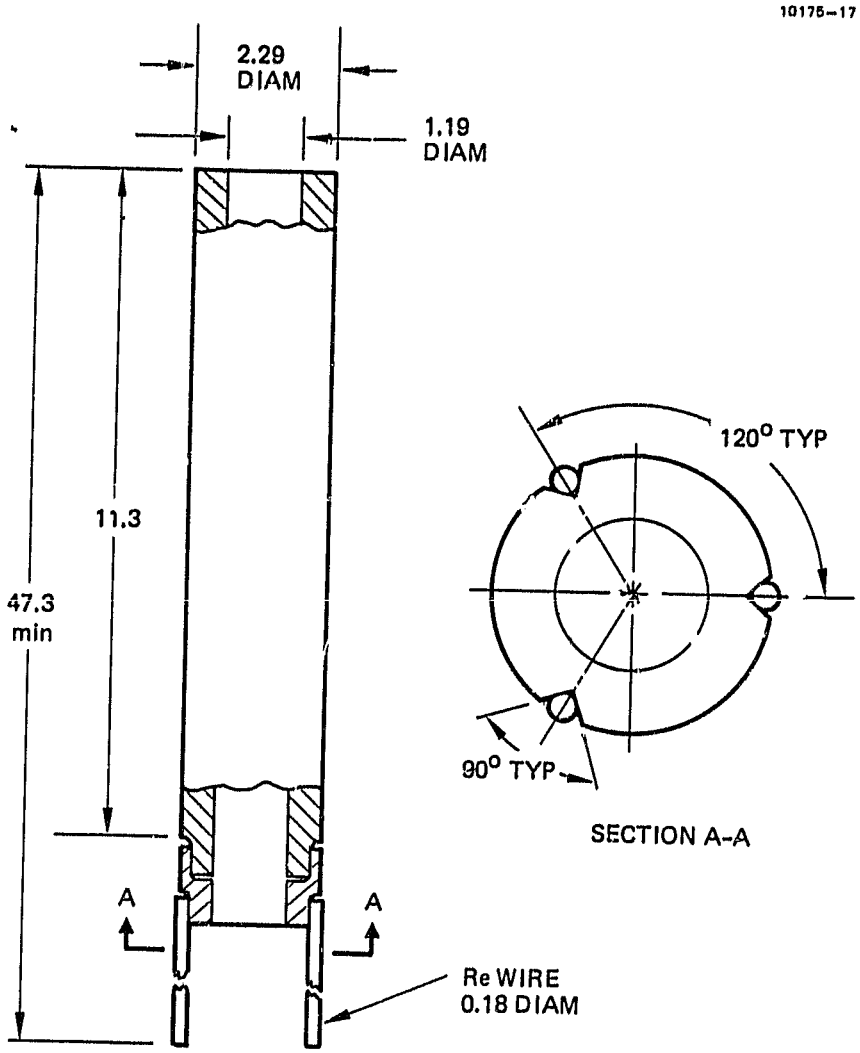

Figure 22. Porous-tungsten cathode insert. Dimensions in mm.

brazed collar and three rhenium wires; these wires are spotwelded to the interior walls of the upstream end of the cathode tube to retain the insert in place. (The insert is positioned in the cathode tube in such a manner that the downstream end of the insert is 0.25 mm upstream of the cathode tip.) This design has a number of attractive features:

1. The insert contains a relatively large amount of emissive material, only a small fraction of which is exposed at the surface.

2. The physical attachment of the insert (spotwelded wires) is remote from the high-temperature emitting zone (at the downstream end), minimizing heat drain.

3. Depleted surface emissive material is naturally replaced by fresh (deeper-lying) material by capillary and diffusion forces.

4. The lifetime properties and handling characteristics of this generic type of insert are well known, and its contamination resistance is well known.

The first of the advantages listed above is equivalent to the observation that very little of the emissive material is simultaneously exposed to the atmosphere; lack of this feature may account for the comparative sensitivity of rolled-foil inserts to atmospheric exposure.

PW inserts are fabricated by the following procedure, details of which are important in achieving satisfactory performance:

1. Porous-tungsten powder is classified according to granule size to achieve a narrow distribution of powder-granule dimensions; the average diameter of the granules is of the order of 4 μm.

2. The material is pressed and sintered to a density near 80% of theoretical; lower-density material (<70%) may have inadequate physical strength, and higher-density material will contain insufficient void volume for the emissive material, and will also contain non-innerconnected pores (i.e., pores which cannot serve as reservoirs for emissive material).

3. The porous material is impregnated with a filler (either plastic or copper) to render it machinable.

4. The material is machined to the correct shape.

5. The machined material is chemically etched to remove surface material that has been smeared by the machining process.

6. The filler material is removed by high-temperature evaporation in vacuum.

7. The collar and support wires are attached by furnace brazing using Mo-Ru eutectic braze.

8. The porous tungsten is impregnated with emissive material, and excess material is removed from the exterior of the insert.

9. The insert is weighed before and after impregnation to assure a 75 to 90% fill of the available pore volume.

Figure 23 shows the effects of deleting or improperly performing the chemical-etching step mentioned above; one of the inserts illustrated has its surface pores smeared almost shut, restricting the external area from which emissive material is available to a very small fraction of the insert surface. The other insert exhibits the open-pore structure of properly etched material. This difference is visible to the unaided eye: the insert with smeared surface material appears shiny, while the properly etched insert appears matte grey.

B. POROUS-TUNGSTEN-INSERT INTEGRATION AND TESTING

In incorporating PW inserts into the EMT, we investigated several specific areas of concern: (1) changes in the thermal profile of the cathode-isolator-vaporizer (CIV) and neutralizer-isolator-vaporizer (NIV) which result from the increased power dissipation of the PW inserts, (2) cathode-ignition requirements, and (3) the lifetime capabilities of cathodes equipped with these inserts.

13867-23

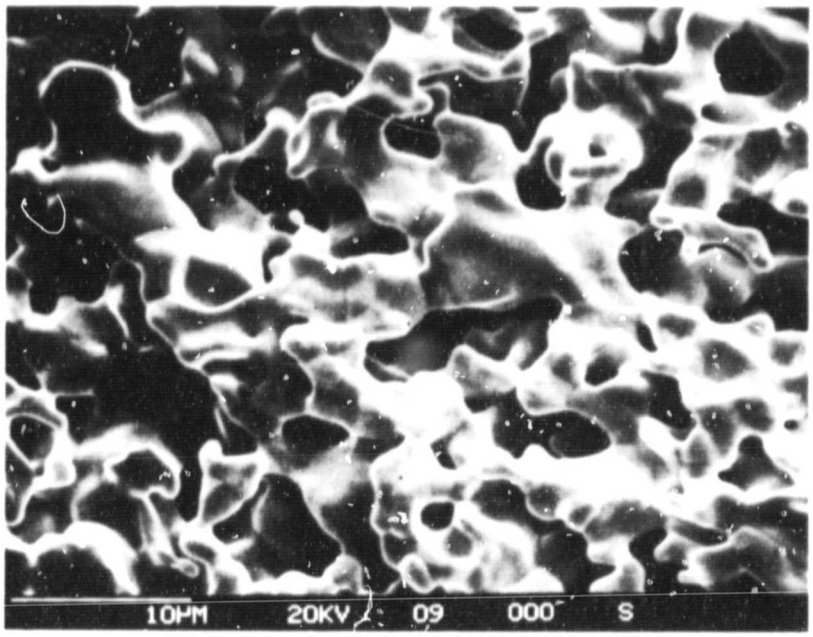

PROPERLY ETCHED POROUS TUNGSTEN

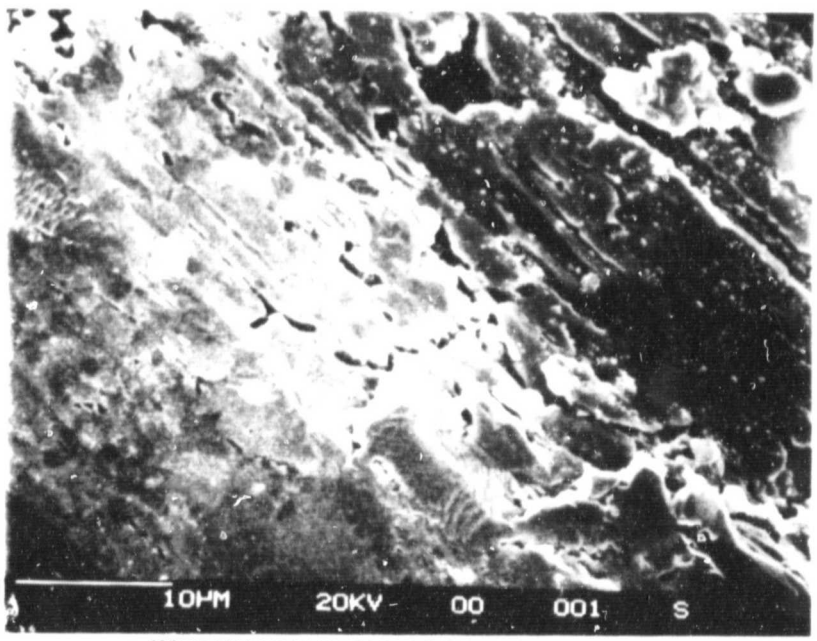

IMPROPERLY ETCHED POROUS TUNGSTEN

Figure 23. Effect of chemical etching on porous-tungsten surface openness.

1. Thermal Design

The new cathode design operates under thermal conditions that differ from the previous design. In particular, initial operation of an EMT equipped with a PW insert indicated a new requirement for the application of cathode heater power during normal operation. This requirement satisfied the need to stabilize discharge operation and maintain adequately low keeper voltages. In the case of the neutralizer, the nominal operating heater-power requirement posed the hazard that the increased amount of heat conducted from the cathode to the vaporizer might result in loss of vaporizer control (i.e., that vaporizer operating temperatures above the nominal operating level could occur even with zero vaporizer input power). This concern led us to develop a thermal model for the NIV structure, which indicated the need for two changes in the NIV structure: reduced thermal conductance between the neutralizer cathode and the neutralizer vaporizer, and increased heat shielding of the neutralizer cathode. Modifications to accomplish these goals include a thinwall cathode tube and a double-layer, thinwall heatshield. These have been successfully incorporated into the FMT design. Figure 24 shows the predictions of the thermal model before and after the revisions. A similar model was also developed for the discharge cathode, and similar modifications have been incorporated in the FMT design. These modifications work very effectively, bearing out the thermal-model predictions, and they bring the additional benefits that (1) higher neutralizer cathode heater power can be used without risk of loss of vaporizer control, (2) the same cathode tip temperature is achieved with less applied tip heater power, and (3) less total thruster input power is required.

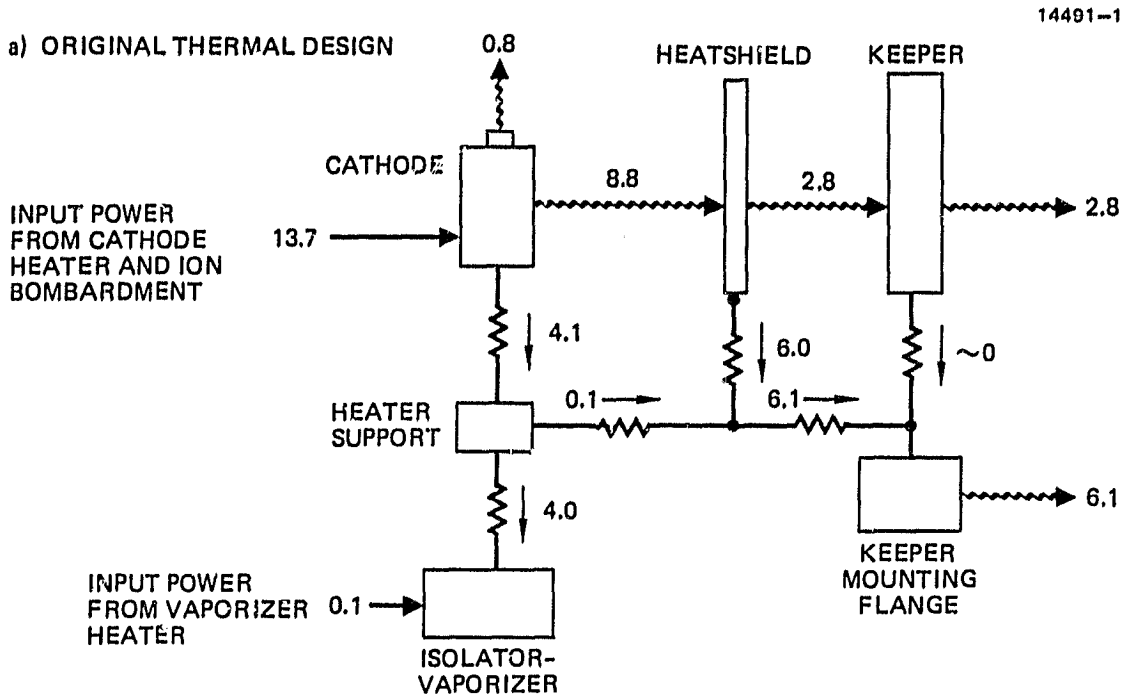

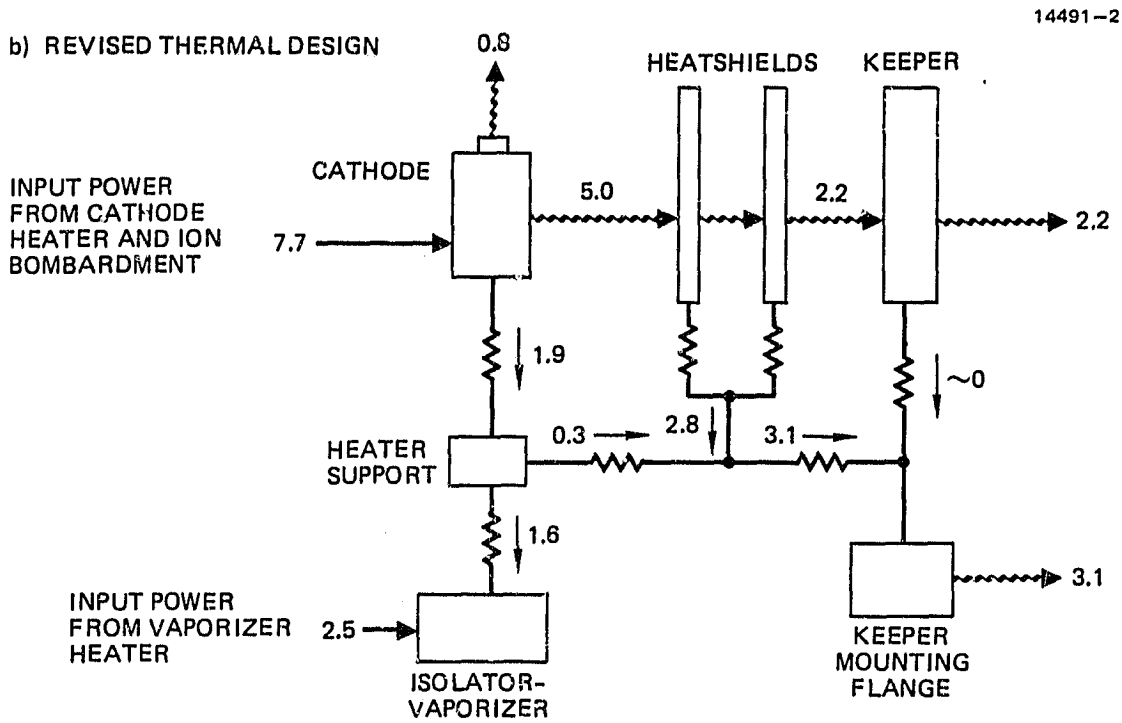

Figure 24. Thermal model predictions for original and revised NIV. Numbers indicate thermal power transfer in watts.

2. Cathode Ignition Tests

Concurrent with the change of cathode insert design from RTF to PW, revisions to the design of the PEU were implemented, incorporating a low-current, high-voltage (550-V, 4-mA) "ignitor" power supply to supplement the normal 50-V keeper supply at the time of ignition. To characterize the ignition capabilities of the new insert design and demonstrate acceptable performance of the revised ignitor circuit, we conducted tests to parametrize the conditions under which cathode ignition was successful. We independently varied mercury flowrate and cathode tip temperature, and mapped the regions of parameter space that gave successful ignition. In addition, we recorded trends in actual ignition voltage (i.e., the maximum voltage reached during the ignition transient, as recorded by a peak-reading voltmeter).

The procedure for conducting these measurements is illustrated in flowchart form in Figure 25. In each case, we attempted ignition first with the low-voltage keeper supply; if ignition was not accomplished, we then tried the high-voltage ignitor supply. The results of these tests are shown in Figures 26 and 27 for conditioned EMT neutralizer and discharge cathodes, respectively. These results helped to define the minimum flowrate and cathode-heater power for successful FMT cathode ignition under low- and high-voltage ignition conditions, as well as the nominal ignition conditions indicated on the figures.

3. Cathode Cyclic Test

In order to characterize the trends in cathode performance which occur with aging, we conducted a cyclic lifetest of discharge and neutralizer cathodes. The cathodes we used for this test were fabricated to the same design as the flight-model cathodes, with thin-wall (127-μm-thick) cathode-tube

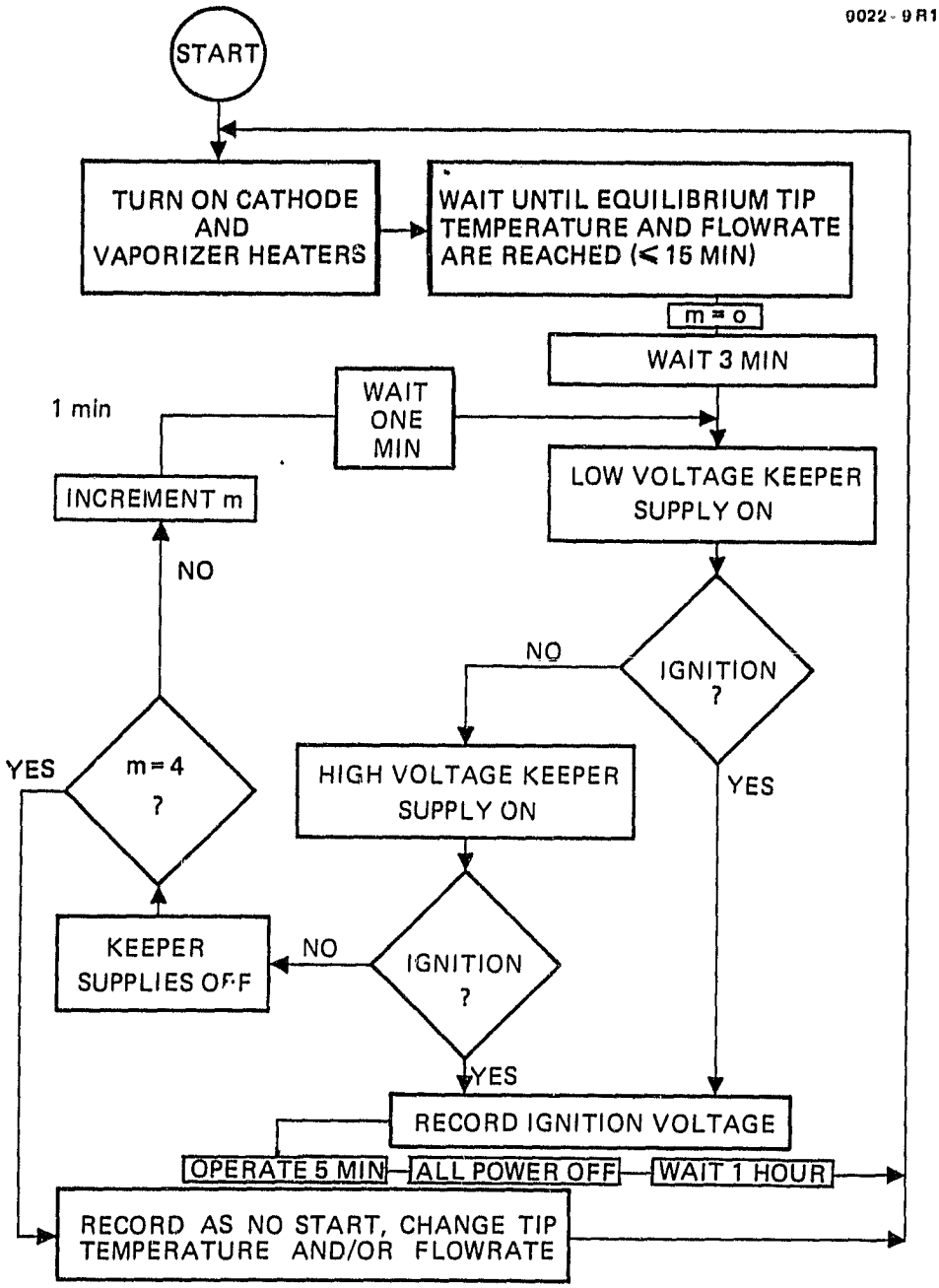

Figure 25. Ignition-test procedure.

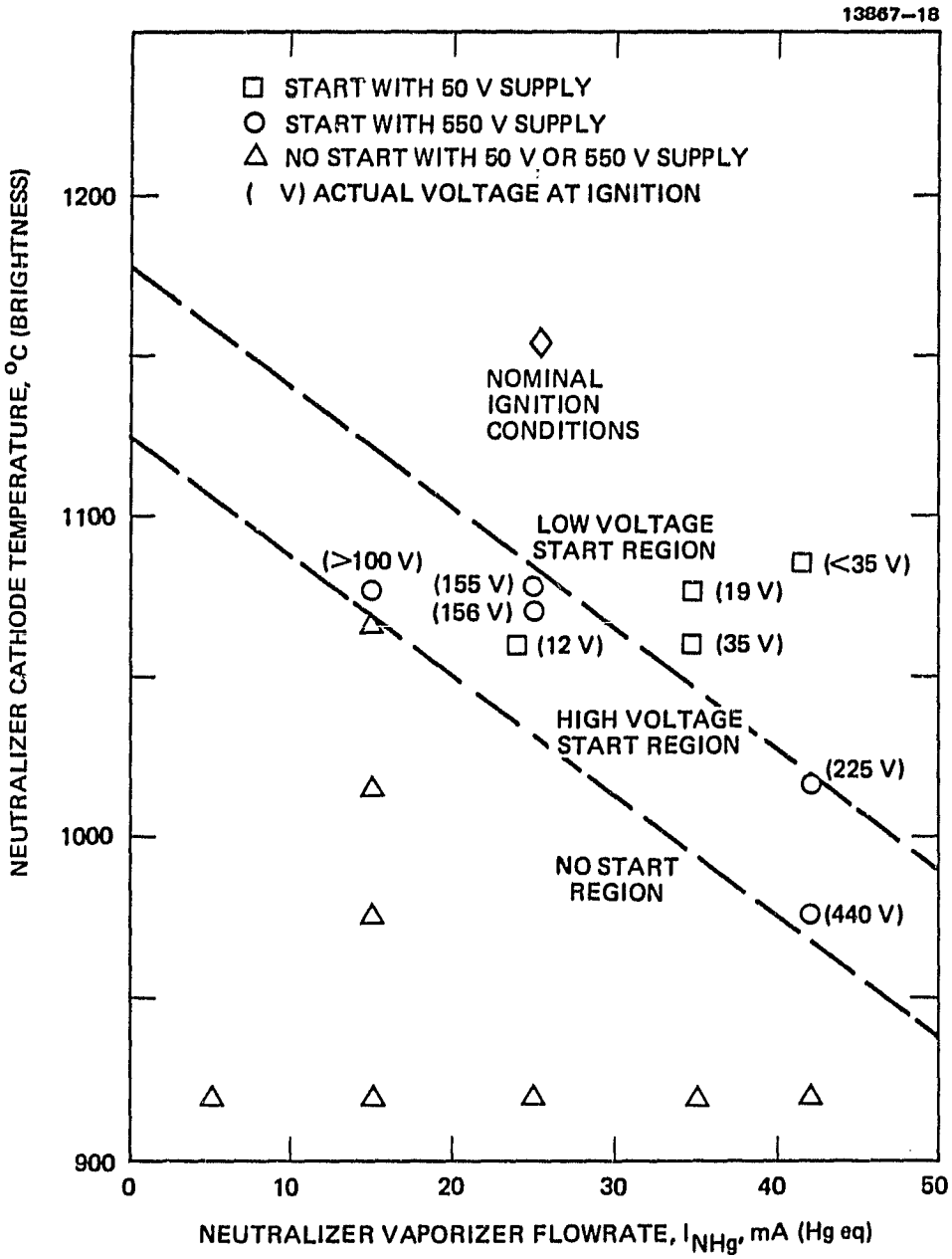

Figure 26. Neutralizer cathode ignition requirements.

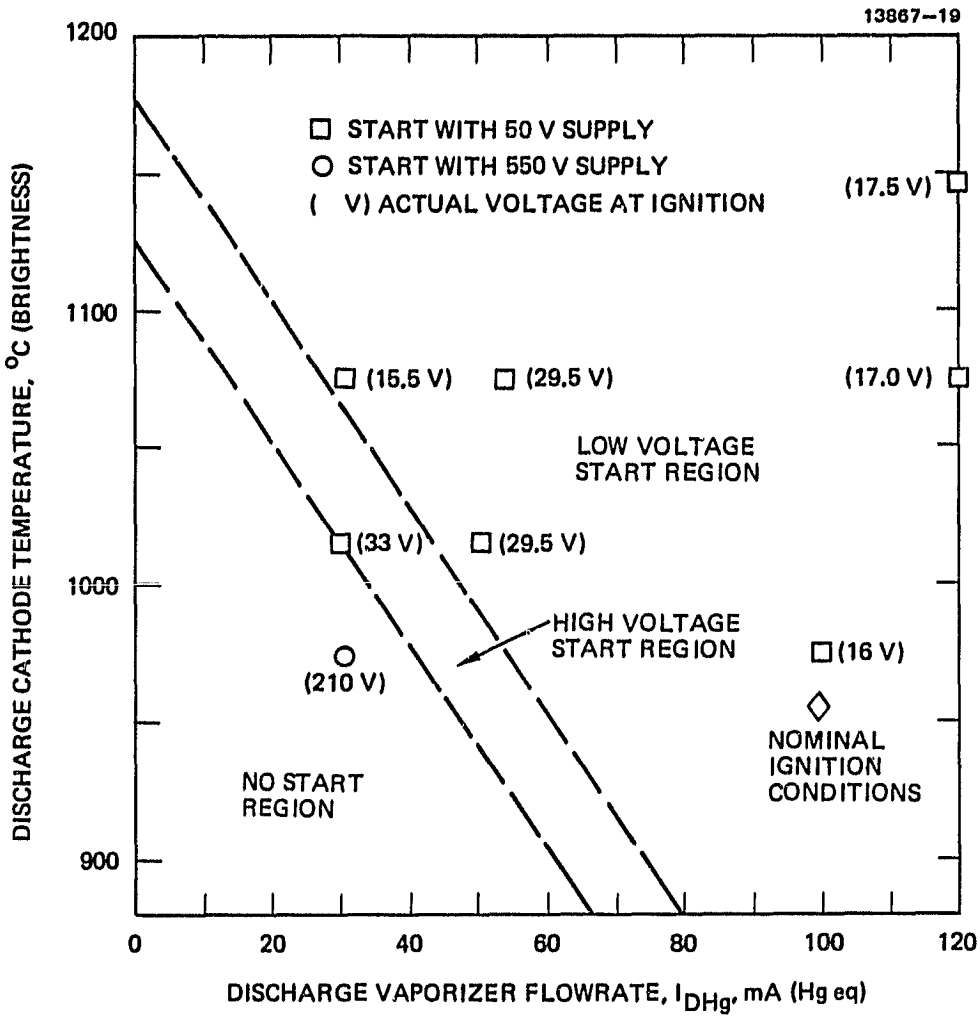

Figure 27. Discharge cathode ignition requirements.

construction, swaged-and-welded cathode tip design, and standard FMT heatshields. The inserts used were built by the same vendor and to the same specifications as the flight cathode inserts. The cathodes were installed in an EMT (complete except for the absence of the accel grid) to produce a valid magnetic-field environment. The accel grid was omitted because no beam extraction was employed, and the higher open area of the accelless extraction system produces a ratio of neutral-loss-rate to plasma-loss-rate that more closely approximates the ratio in a thruster with beam extraction.

Figure 28 illustrates the test arrangement schematically. A microcomputer was used to control the cyclic testing, employing software which was intended to approximate the action of the IAPS DCIU cathode-ignition software. Figure 29 is a flowchart of the algorithm that was used to conduct the cyclic testing. The attempt in this algorithm was to closely simulate the IAPS cycle of 2.76 hr "on" and 2.00 hr "off", where "off" includes startup time. Figures 30 and 31 show the discharge and neutralizer-keeper voltages as functions of cycle number during the test. The test was begun with discharge-cathode-heater power of 2 W (the nominal IAPS flight value at setpoint 0) during steady-state operation. This value was raised to 3 W after early cycling revealed an increasing keeper voltage. An occurrence of a facility pressure excursion is also shown in Figure 30. The cathodes were reconditioned following this pressure excursion, but the discharge-keeper voltage persisted at an elevated value.

The results of the cyclic testing reveal significant variation in the discharge and neutralizer keeper voltages, but this variation is well correlated with facility pressure excursions and changes in operating conditions. We interpret these test results to indicate that the total accumulated operating duration was insufficient to reveal any long-term changes in cathode performance due to operating time or startup cycles.

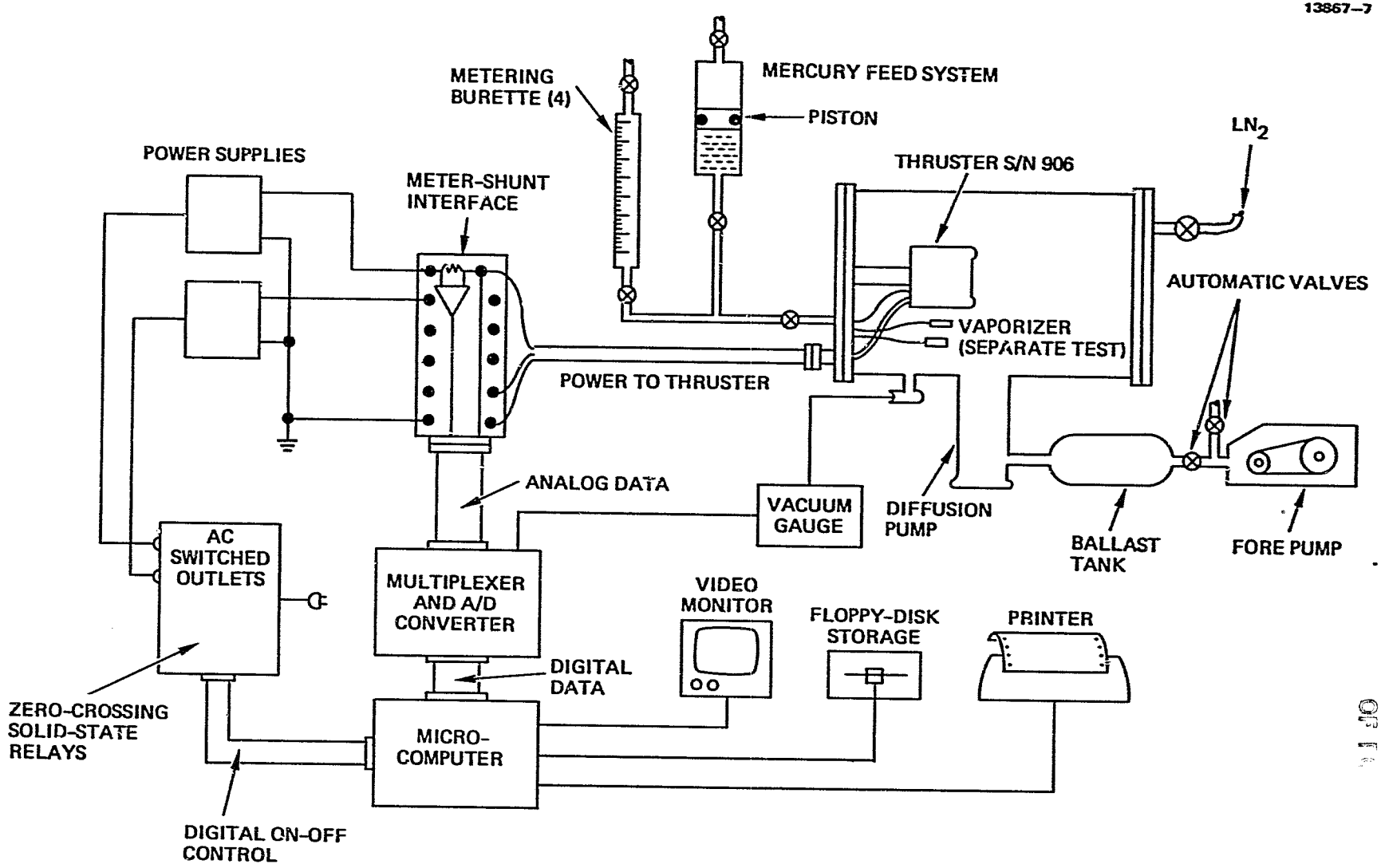

Figure 28. Schematic of cyclic testing apparatus.

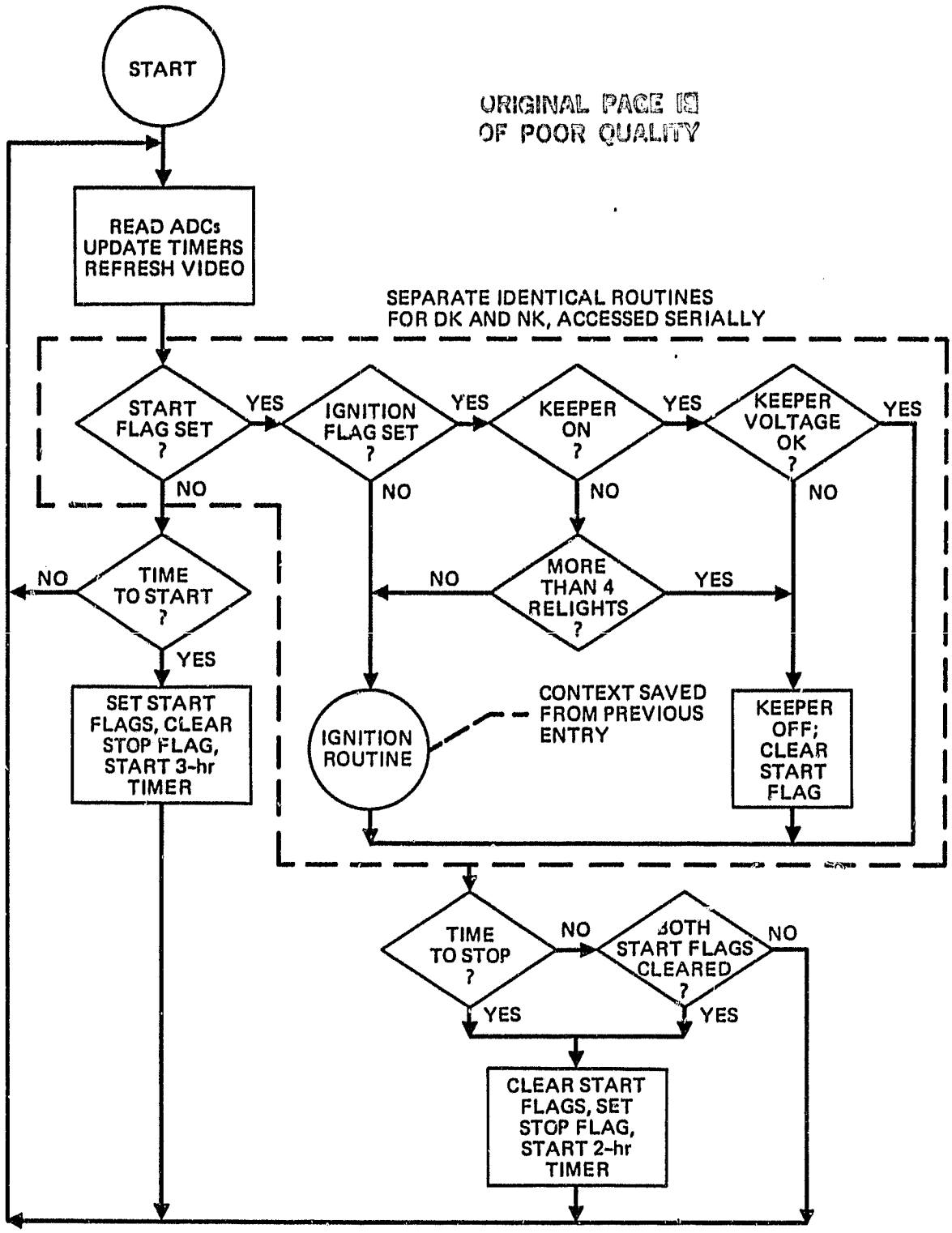

Figure 29. Flowchart of cyclic test operation.

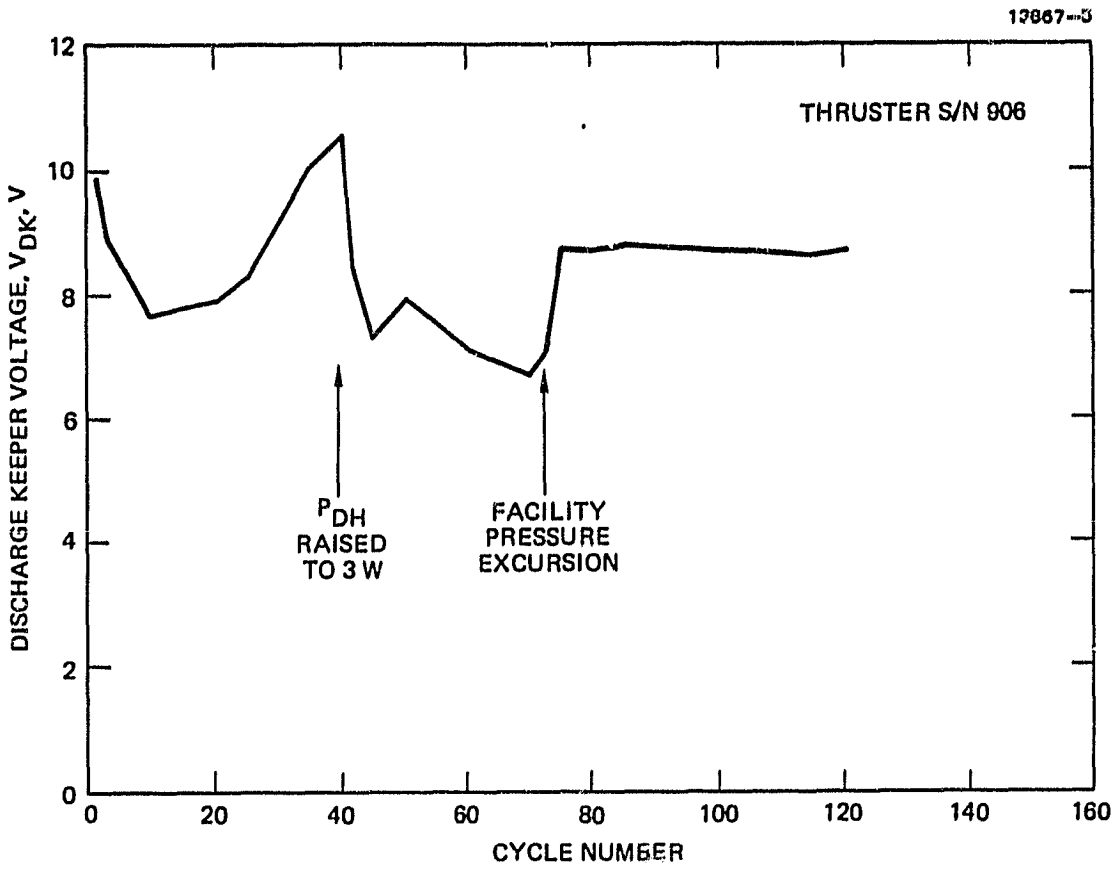

Figure 30. Discharge keeper voltage during cyclic lifetest.

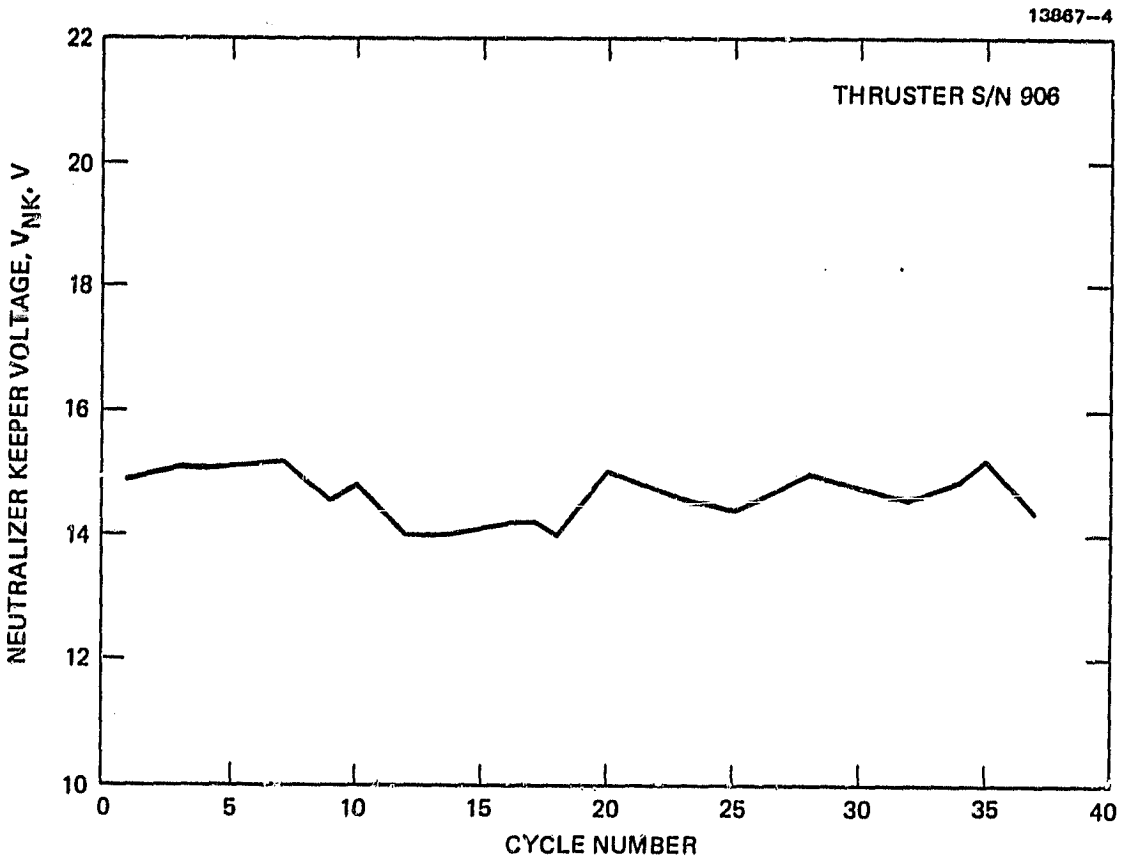

Figure 31. Neutralizer keeper voltage during cyclic lifetest.

The discharge-keeper voltage in this test was significantly lower than that during previous tests of complete EM thrusters under nominal operating conditions. It is possible that the absence of beam extraction in the cyclic lifetest was responsible for this difference.

SECTION 7

VAPORIZER CHARACTERIZATION

The porous-tungsten vaporizer is the heart of the propellant feed system of the 8-cm thruster; it must possess a reproducible flowrate-vs.-temperature characteristic, and it must undergo a very large number of thermal cycles without permitting liquid-mercury intrusion or leakage. In the testing of vaporizers early in the IAPS flight program, vaporizer problems occurred which we ultimately determined to have resulted from insufficiently pure mercury. These problems have now been eliminated by the use of ultrapure mercury and by employing handling procedures which assure that the mercury will not be exposed to materials which could amalgamate with it. We conducted lifetests of vaporizers using the ultrapure mercury and the new handling procedures and found no shift in vaporizer calibration.

Figure 32 shows the downstream (vapor-side) surface of a discharge vaporizer; a white flaky contaminant residue is visible on the interior porous-tungsten surface of the vaporizer. We have concluded that the white residue consists of contaminants in the mercury that were transported through the pores of the porous tungsten over a time period shorter than the 50-hr duration of the acceptance test conducted at 350°C and 410 kPa (60 psia), to which all new vaporizers are subjected. This contamination produced a shift in the flowrate-vs.-temperature calibration of the vaporizer, as shown in Figure 33. Intrusion testing of this vaporizer revealed that liquid mercury would completely penetrate the vaporizer at pressures and temperatures well below those present in routine operation. In one case, a vaporizer having an intrusion pressure of 780 kPa (114 psia) at 350°C before the 50-hr

13867-24

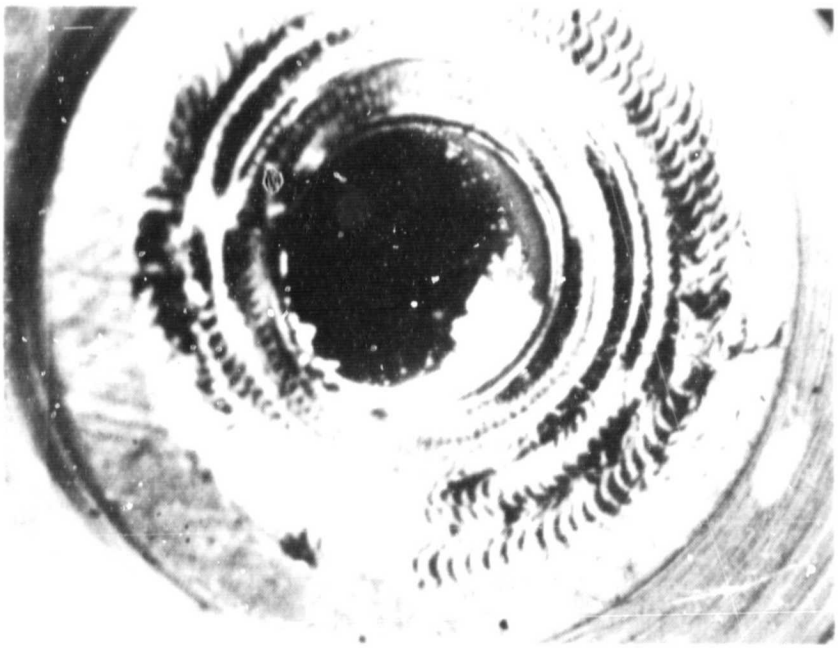

VAPOR END OF VAPORIZER (16X)

DEPOSITS (230,000X)

Figure 32. Discharge vaporizer, showing contaminants.

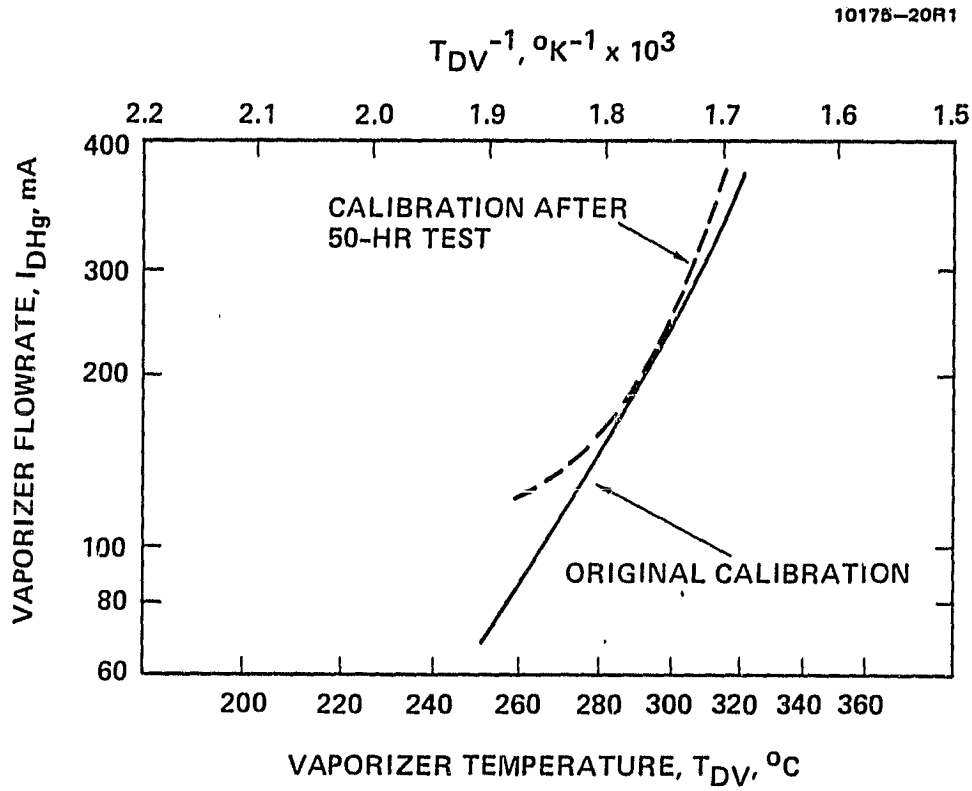

Figure 33. Vaporizer calibration, showing effect of contamination.

test intruded spontaneously during the test, leaking liquid mercury through the porous tungsten. This test was conducted at the standard pressure of 410 kPa (60 psia).

Analysis of the white residue revealed that it consisted largely of silver and gold, which are the dominant residual elements in the 99.9938% pure mercury that was used for the testing. Calculation shows that the quantity of impurities in this mercury (which amount to 62 parts per million) are sufficient to coat the pores in a vaporizer plug, reducing the intrusion resistance of the material. In subsequent testing, mercury of 99.99999% purity was employed, and the contamination-related problems have not recurred. This ultrahigh-purity mercury is used in the flight thrusters, and calculations indicate that with this mercury, no contamination problems should occur within the nominal lifetime of the thrusters. Figure 34 shows the original calibration characteristic of a vaporizer that was subsequently contaminated to the point of intrusion. This vaporizer was then baked out in vacuo and operated for over 50 hr with the ultrapure mercury. The calibration data obtained after this testing fall on the same curve as the original (pre-contamination) calibration data.

The results of these tests indicate that great care must be taken to assure that mercury propellant is free of amalgamated impurities; such impurities gradually coat the interior surfaces of porous-tungsten vaporizers, reducing the resistance to liquid-mercury intrusion, and altering the relationship between vaporizer temperature and mercury flowrate (the vaporizer calibration characteristic). We do not fully understand the process by which amalgamated impurities are deposited on the vapor side surfaces of vaporizers, but we have clearly demonstrated that the use of mercury with a sufficiently low impurity content eliminates problems of intrusion and altered calibration.

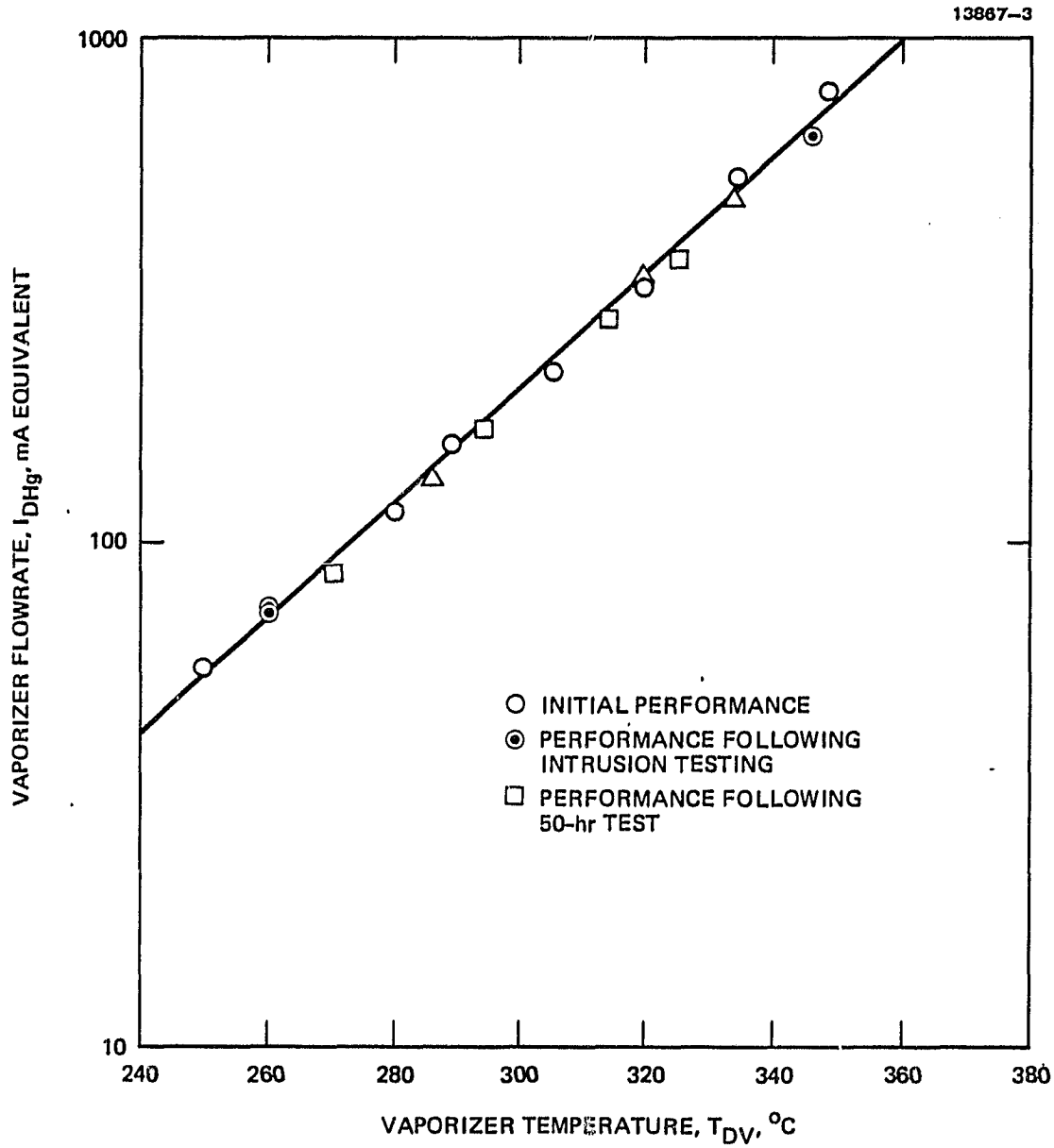

Figure 34. Vaporizer calibration curve, showing absence of shift after testing.

SECTION 8

THRUSTER ENVIRONMENTAL INTERACTION

Three forms of environmental interaction are of concern for a thruster system that will be launched and operated in space. One concern is the hazard to the thruster that is posed by contaminants originating in/from the launch vehicle and from spacecraft outgassing. Another concern is the interference hazard to the spacecraft that is posed by thruster-system electrical-noise emissions. A third concern is that the thruster withstand the launch-vibration environment without incurring mechanical damage. To investigate the first concern, we conducted a study of potential contaminants and their likely interaction with the thruster. To address the second concern, we directly measured the radiated and conducted emissions of an operating thruster system, using standard procedures for electromagnetic interference (EMI) measurement. Finally, we conducted vibration tests of EMTs and incorporated design changes to improve resistance to vibration. Comprehensive reports detailing each of these topics have previously been provided to the NASA LeRC Technical Project Manager; we provide only summary information here.

A. CONTAMINATION HAZARDS TO THE IAPS THRUSTERS

We have reviewed literature pertaining to contamination hazards to the IAPS thrusters and whenever possible we have checked the calculations for the predicted deposition levels and concentrations of contaminants. We conclude that the most significant vapor and gaseous hazards are excessive prelaunch humidity and postlaunch deposition of volatile condensible material (VCM). Excessive prelaunch humidity poses a hazard to

the cathode inserts; since the emissive material that is contained in the pores of the inserts is hygroscopic, it could swell and fracture the insert if exposed to sustained high humidity, or this could happen in space on initial conditioning of the cathode. Even if the insert survives structurally, it may be permanently or temporarily poisoned by the water vapor exposure to an extent that seriously compromises subsequent cathode starting and operation. Condensing VCMs could form insulating films on critical conductive thruster surfaces. These two hazards originate from the ambient prelaunch environment and from postlaunch outgassing of organic material, respectively.

The remaining hazards examined in our study were found to be less worrisome. The predicted density levels of reactive VCM are low enough that they do not appear to pose a threat. Also, no significant deposition levels of conductive VCM or conducting/insulating nonvolatile residue (NVR) are expected. This study has addressed only contaminants which are deposited in vapor form; particulates and macroscopic contaminants were not considered.

Our calculations show that the worst-case VCM deposition thickness during the first year of the nominal mission (i.e., nominal altitude and temperature profile) lies between 6.4 nm and 35 nm, depending on specific assumptions. More sophisticated calculations (i.e., computer modeling) would be required to narrow these bounds (which are based on elementary calculations). In addition, actual testing with a thruster would be required to determine if contaminant layers of the thickness mentioned above would compromise thruster operation. We anticipate that the principal hazard presented by this type of contamination would consist of discharge-ignition failure caused by the presence of an insulating contaminant layer on the anode.

To evaluate the magnitude of the water-vapor hazard, we conducted a test in which we exposed an 8-cm thruster neutralizer cathode to the projected worst-case water-vapor level and duration (55% relative humidity at 25°C for 8 hours). We conditioned the cathode by the standard procedure and characterized its performance, both before and after the exposure. Our test results showed the presence of only a small (0.5-V) increase in keeper voltage as a result of the exposure. These results are plotted in Figure 35. From the results, as well as the satisfactory starting charateristics of the cathode after exposure and reconditioning, we conclude that expossure of the thruster to the specified water vapor limits poses no structural hazard to the cathode inserts and may cause at worse only a minor degradation in cathode performance.

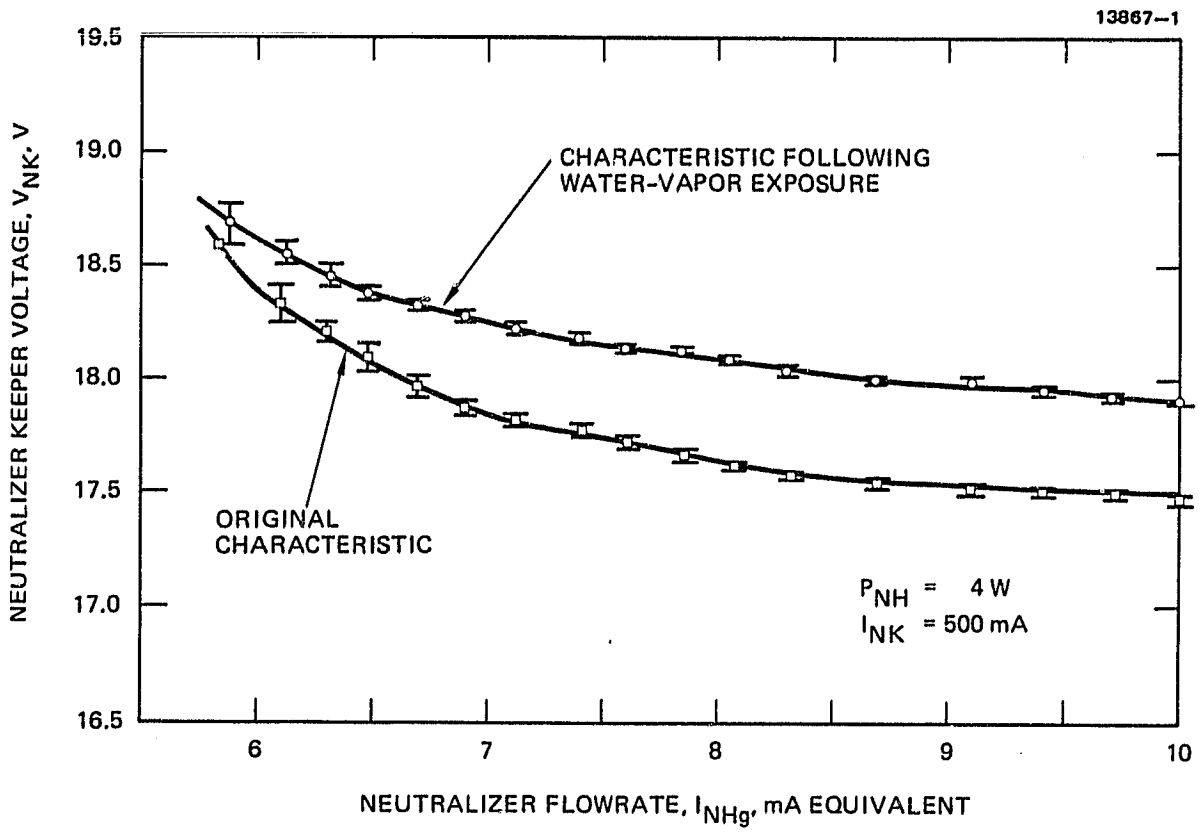

Figure 35. Effect of water-vapor exposure on neutralizer performance.

B. EMT ELECTROMAGNETIC INTERFERENCE MEASUREMENTS

In order to characterize the electromagnetic interference (EMI) generated by the EMT, PEU, and DCIU, we conducted tests to measure both conducted and radiated EMI. We conducted these tests with reference to the relevant MIL standard (MIL-STD-461A); however, the radiated EMI measurements were necessarily nonstandard since they were made in a metal vacuum chamber, rather than an anechoic chamber. This measurement technique has the likely effect of making the test results upper bounds on radiated field intensity because of finite reflection from the chamber walls. The measurements were conducted with engineering-model electronics (PEU and DCIU). The DCIU was commanded via a ground-test console from which hexadecimal commands could be entered and IAPS telemetry signals received and displayed, simulating the exchange of time-tagged commands and telemetry with the spacecraft.

The data presented in Table 5 are the worst-case test results from the conducted-EMI measurements (i.e., CE03 test procedure), carried out during thruster operation in most of the Table 3 modes. The connection points used for these measurements were the power, command, and telemetry lines corresponding to the same lines in the interface between the IAPS flight package and the spacecraft. For our tests, the ground-test console simulated the spacecraft. We recorded both broad- and narrow-band thruster emissions over the frequency range from 0.02 to 50 MHz for the conducted EMI.

Radiated EMI measurements were made using a microwave horn antenna; this antenna was mounted at a constant radial distance from the thruster on a curved track inside a 1.2-m-diameter vacuum chamber. The antenna could be moved (from outside the vacuum chamber) to various azimuthal positions around the thruster and was always oriented so that it pointed toward the thruster grid system. We recorded narrow-band radiated emissions over the frequency range from 0.8 to 10 GHz, with the

thruster in steady state operation in the Table 3 modes. We also measured broad-band emissions at the spacecraft communication frequencies of 1.65 and 1.77 GHz during thruster transients. Both transient and steady-state emissions were recorded with the antenna at positions of 0, 45, and 90° relative to the thrust axis. These tests showed that the radiated emissions from the thruster were very low-level and often were below the detection threshold of the instrumentation; this statement applies even to the 0° case in which the antenna was actually on the thruster beam axis. Table 5 lists worst-case results from the radiated-EMI tests.

C. VIBRATION TESTING

We conducted four separate vibration tests of EMTs to flight qualification levels for the IAPS Shuttle-launch in order to evaluate the vibration worthiness of the EMT design at various stages of evolution. The paragraphs below list the failures and problem areas that were identified following each test, and the the corrective measures taken. These measures were processed through failure reports and design changes which are now reflected in the flight-thruster documentation (mechanical drawings and Internal Process Documents). In the last test, we recorded data from a number of accelerometers that were fitted to the thruster; these data were subsequently analyzed by a standard Hughes numerical routine.

Vibration Test of Thruster S/N 904

This standard EMT suffered a single failure as a result of vibration testing, and five additional problem areas were identified.

Table 5. Worst-Case EMI Test Results

TYPE OF MEASUREMENT	VOLTAGE LEVEL
• Conducted (CE03)	
Steady State	+31 dB over specified limit
Transient*	+12 dB over specified limit
• Conducted (CE04)	
Steady State	+29 dB over specified limit
Transient	+34 dB over specified limit
• Radiated	
Steady State	+49 dB μV/m
Transient	+61 dB μV/m/MHz

*The only CE03 transient signals measured occurred during a simulated screen-to-accel arc and a simulated grid clear operation. Both simulations involved arcs external to the vacuum chamber, and they may be nonrepresentative of conducted EMI that would be experienced under thruster operating conditions.

1. Failure: Broken RTD lead.

   Action: New RTD design and revised mount incorporated.

2. Problem: NIV feed tube notched by contact with NIV bracket.

   Action: Increased clearance for feed tube to eliminate contact with bracket.

3. Problem: Sharp screw ends in gimbal tube abraded wiring harness.

   Action: Used shorter screws with rounded ends; removed excess length from wiring harness.

4. Problem: Broken spotwelds on coaxial-lead tiedown.

   Action: Replaced with nut-and-bolt tiedown.

5. Problem: Bent neutralizer-keeper bracket.

   Action: Used spacers on bracket screws to remove torque from bracket.

6. Problem: Loose screws in several places.

   Action: Improved quality control (thruster was not assembled to flight specifications).

Vibration Test of Thruster S/N 902R

The "R" in the serial number of this thruster identifies it as a retrofitted thruster, i.e., an EMT that had been revised to incorporate flight-thruster design modifications. This vibration test revealed four new problem areas:

1. Problem: Broken sheath on neutralizer cathode heater lead.

   Action: Heater-lead support added.

2. Problem: Broken wire on neutralizer switch.

   Action: New handling procedure defined to minimize number of flexures of wires; heat-shrink strain relief added.

3. Problem: Binding and interference problems in the gimbal.

   Action: Special design-and-test effort to assure absence of binding or excessive looseness in the gimbal.

4. Problem: Cracked feedthrough insulator on rear shield.

   Action: Insulators redesigned to eliminate stress-concentration near vent hole.

Vibration Test of Thruster S/N 903R

This vibration test actually consisted of two tests: In the first test, a bracket which attaches the gimbal-tube yoke to the gimbal actuator shaft fractured, causing the thruster to undergo large amplitude motions about its remaining attachment point (the test was terminated immediately after the onset of this motion). We later determined that the broken bracket was of an obsolete design and had been inadvertently installed in the gimbal assembly. The bracket was replaced with one of the current design, and the test was repeated successfully.

The only anomaly that was observed following the test was that the neutralizer-cathode insert could be caused to rattle against the interior of the cathode tube on gentle shaking of the thruster. This probably resulted from breakage of the spotwelded attachment of one the three legs which position the insert in the cathode tube. The spotweld failure, which did not alter the neutralizer performance measurably, may have occurred when the original gimbal bracket failed. No corrective action was taken because of this anomaly.

SECTION 9

THRUSTER DESIGN DOCUMENTATION

During the course of the Flight Program and the contractual effort here described, a substantial number of design changes were made to the thruster and associated mechanical components. In many cases, these design changes resulted from technology developments which are described in the present report. These include changes to improve vibration resistance, improved material specifications (such as for the porous tungsten vaporizers and cathode inserts), and improved processing methods (as in the case of the flame-spray techniques employed in fabricating the cathode heaters). The documentation of these design and process changes for the IAPS flight thruster fabrication was inadequate to define the flight design so that thrusters could be reproducibly built to it, independently of the skilled personnel who built the flight thrusters. To bridge this documentation gap, we undertook an effort under this program to upgrade the drawings and process documents so they were complete, definitive, and self-consistent, reflected the final flight-thruster design, and were organized in a useful fashion with a drawing list. This work was completed, and a complete set of flight-thruster documentation was generated and forwarded to the NASA LeRC Technical Project Manager.

SECTION 10

CONCLUSIONS

This program has fulfilled a vital need in providing the necessary technology support for the IAPS flight program. Work conducted under this program has elucidated the critical component and system characteristics defining acceptable performance and successful operation of the IAPS flight system. The principal accomplishments under the program have been:

- Definition of design specifications to assure stable operation of the thruster/ power-processor combination.
- Integration of porous-tungsten cathode inserts into the EMT to provide required lifetime and reproducibility of operation.
- Determination of requirements to assure reliable and reproducible long-term operation of porous-tungsten vaporizers.
- Specification of critical design features of EMT components to assure standardized performance, adequate lifetime, and the required vibration resistance.
- Definition of algorithms for the control and fault correction of the IAPS flight thrusters, based on experience with the EMT.

Further work identified in this program which should be carried out to complete the IAPS technology development includes: additional investigation of the nature of the thruster/power-processor interaction (and the stability consequences of that interaction); and work to specify how the existing IAPS control software can best accomodate the effects of aging and/or contamination on thruster performance.